of pcDNA3.1-EP4, 250 ng of pGL3-PSAp-Luc, and 5 ng of pTK-RL using Lipofectamine 2000 reagent. After 24 h of incubation, the medium was changed to create androgen-depleted conditions and the cells were incubated again for 24 h. The luciferase activity of the cell lysate was measured using the Dual-Luciferase Reporter Assay System (Promega) with a luminometer (MicroLumat Plus LB96V, Berthold Technologies) in triplicate.

cAMP assay. Cells were seeded at 1.0×10^5 per well in 96-well plates and incubated for 24 h. Cells were washed once with PBS and cultured for 1 h in androgen-depleted conditions. The intracellular cAMP concentrations were assayed using the cAMP-EIA kit (RPN225; Amersham-Pharmacia Biotech) in duplicate. ONO-AE3-208 was added 10 min before the assay.

Statistical analysis. The data were expressed as mean ± SD and their statistically significant differences were determined by one-way ANOVA. Age, serum PSA levels, Gleason sums, and tumor volumes were compared by the Mann-Whitney *U* test, and EP4 staining levels were compared by the χ^2 test. Statistical analyses were all performed using SPSS software.

Results

KUCaP-2 is an androgen-dependent prostate cancer xenograft harboring wild-type AR, producing PSA, and developing castration resistance without AR mutation. Tumor tissues used for the establishment of KUCaP-2 were histologically diagnosed as prostate cancer based on positive AR and PSA immunohistochemistry staining (Fig. 1A). Western blotting analysis revealed that KUCaP-2 cells expressed AR and PSA (Fig. 1B). In mice, the KUCaP-2 tumor regressed soon after castration and reproducibly regrew after 1 to 2 months. Sequence analysis of *AR* in KUCaP-2 tumors before and after castration showed no *AR* mutation.

Xenograft tissues of KUCaP-2 were transplanted into 12 mice and collected during androgen-dependent growth (AD), castration-induced regression nadir (ND), and castration-resistant regrowth (CR) stages (n = 4, each; Fig. 1C). The tumor volumes were 3,012 ± 467, 562 ± 208, and 1,962 ± 560 mm^3, and the median PSA values of the mice were 166.0, 4.0, and 50.9 ng/mL for the AD, ND, and CR stages, respectively. There was no histologic difference among KUCaP-2 tumors of each stage (Fig. 1D, a–c). The nuclear expression levels decreased from the AD stage to the ND stage, indicating that the depletion of circulating androgen suppressed nuclear expression of AR in KUCaP-2 tumors at the ND stage. Nuclear expression recovered at the CR stage to levels similar to those at the AD stage (Fig. 1D, d–f).

EP4 expression was upregulated with the progression of castration resistance in KUCaP-2 tumors. To elucidate the mechanisms responsible for the development of castration resistance, we evaluated the gene expression profiles of tumors at each stage using DNA microarray analyses. In total, for 2,476 genes, there was a significant difference ($P < 0.05$) in expression between at least two stages. The *k*-means clustering (k = 10) of these genes was performed to select candidate genes (Fig. 2A). Previous reports on DNA microarray analysis in several different xenograft models showed that *AR* was the only gene consistently upregulated during castration-resistant progression (10). In our study, *AR* expression slightly increased from the AD stage to the ND stage (ratio = 2.7, P = 0.006), with no difference between the ND and CR stages (ratio = 1.1, P = 0.280). The *PSA* expression of tumors slightly and not significantly decreased from the AD stage to the ND stage (ratio = 0.6, P = 0.138) and recovered at the CR stage. To find genes associated with castration resistance, we explored genes in the cluster whose expression levels were low in both the AD and ND stages but high in the CR stage. Among 111 genes in this cluster, the CR/ND ratio of *EP4* expression was the highest (ratio = 15.7, P = 0.029; Table 1). These results were validated by real-time PCR analysis (Fig. 2B). Moreover, *EP4* expression was higher in the androgen-independent cell lines (DU145, PC3) compared with an androgen-dependent cell line (LNCaP; data not shown), consistent to other reports (11–13).

EP4 expression was higher in clinical CRPC than in HNPC. EP4 was mainly expressed in cellular membranes or in the cytoplasm of KUCaP-2 tumor cells, with more expression at the CR stage compared with the AD stage (Fig. 2C, a,b). Using KUCaP-2 samples from CR and AD stages as positive and negative controls, respectively, staining intensity of EP4 in clinical materials from 27 HNPC and 31 CRPC patients was graded (Fig. 2C, c–f). The characteristics of these patients were shown in Table 2. All the CRPC patients had PSA relapse. The serum PSA level and the Gleason sum were higher in CRPC than in HNPC. The EP4 expression level was significantly higher in CRPC than in HNPC (P = 0.0001).

EP4 overexpression induced castration-resistant progression of LNCaP cells through AR activation. We examined whether EP4 overexpression induced castration-resistant progression using LNCaP. LNCaP cells were stably transfected with pcDNA3.1-EP4, and two monoclonal EP4-overexpressing LNCaP clones were established and named LNCaP-EP4(A) and LNCaP-EP4(B). The EP4 signal activates adenylate cyclase, which results in acceleration of the production of cAMP (14). The intracellular cAMP concentrations, PSA expression levels, and cell proliferation ratio of LNCaP-EP4 without androgen were higher compared with those in vector alone–transfected LNCaP (LNCaP-mock) cells, indicating that overexpressed EP4 protein activated adenylate cyclase and induced PSA expression and cell proliferation without androgen (Fig. 3A).

To examine whether AR activation is associated with androgen-independent PSA expression and cell proliferation in LNCaP-EP4, AR expression was attenuated using a stealth RNAi system. PSA expression without androgen was suppressed more significantly by the attenuation of AR in LNCaP-EP4 cells than in LNCaP-mock cells. Further, the suppression of androgen-independent cell proliferation was statistically significant in LNCaP-EP4 cells, but not in LNCaP-mock cells, indicating that AR activation was associated with androgen independence of LNCaP-EP4 cells (Fig. 3B). We examined the effect of EP4 on AR activation using

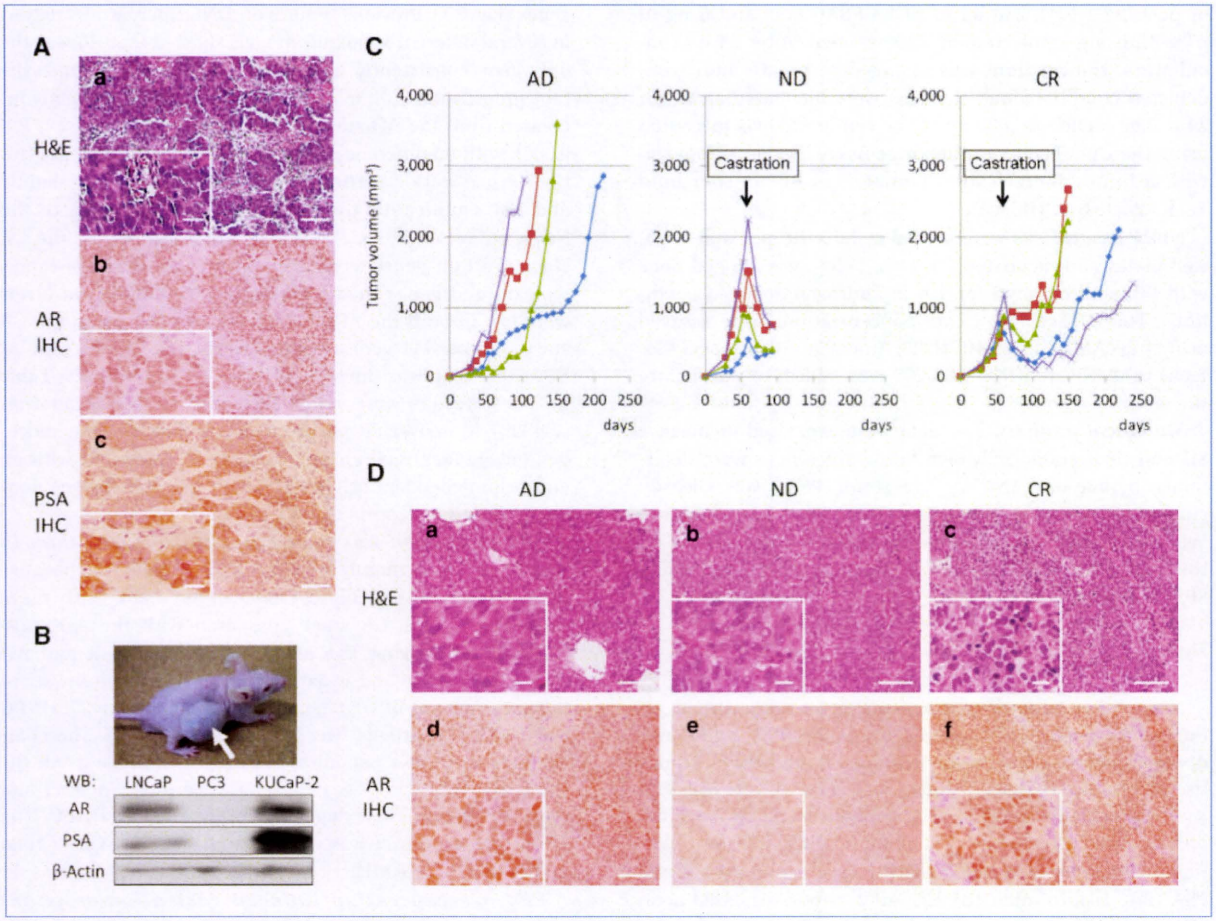

Figure 1. KUCaP-2, a novel established prostate cancer xenograft expressing AR and PSA, regresses after castration of mice and develops castration resistance with nuclear expression of AR. A, H&E staining (a), AR immunohistochemistry (IHC; b), and PSA immunohistochemistry (c) of tumor tissues used for the establishment of KUCaP-2. Scale bars, 50 μm, inset 5 μm. B, KUCaP-2 tumor (arrow, top) expressing AR and PSA detected with Western blotting (WB; LNCaP and PC3 presented as a positive and negative control; bottom). C, the sequential changes in xenograft tumor volume of KUCaP-2 before the tumor extraction at the AD, ND, and CR stages (n = 4 each). D, H&E staining (a–c), AR immunohistochemistry (d–f) at AD, ND, and CR stages of tumors. Scale bars, 50 μm, inset 5 μm.

a luciferase reporter assay in LNCaP cells. EP4 signaling promoted AR activation without androgen to ~50% of the level achieved with androgen stimulation and did not induce additional AR activation in the presence of androgen. Then, we examined whether the increase in cAMP levels and the acceleration of PKA activity was associated with AR activation. PSA expression in LNCaP cells without androgen was induced by both forskolin and dbcAMP but was inhibited by H-89 (Fig. 3C). These results indicate that the signal activation of EP4-cAMP-PKA-AR axis is associated with the castration resistance of LNCaP cells.

The castration of mice decelerated xenograft tumor growth in LNCaP-mock cells but not in LNCaP-EP4 cells (Fig. 3D). The serum PSA values of castrated mice bearing LNCaP-EP4 xenografts were significantly higher than those of mice bearing LNCaP-mock xenografts (median PSA at sacrifice: 4.0 and 32.5 ng/mL in LNCaP-mock and LNCaP-EP4 cells, respectively, $P < 0.05$). These results show that EP4 overexpression induces castration-resistant progression of LNCaP cells *in vivo*.

EP4 antagonist suppressed castration-resistant progression of LNCaP-EP4 and KUCaP-2 tumors. ONO-AE3-208 is an EP4-specific antagonist (5). The Ki values of ONO-AE3-208 for the prostanoid receptors are 1.3, 30, 790, and 2,400 nmol/L for EP4, EP3, FP, and TP, respectively, and >10,000 nmol/L for the other prostanoid receptors (15). To examine the EP4 antagonistic effect of ONO-AE3-208 on LNCaP-EP4 cells, intracellular cAMP concentrations were examined under a variety of ONO-AE3-208 concentrations in androgen-depleted conditions, indicating that 10 to 100 nmol/L of ONO-AE3-208 is sufficient to antagonize overexpressed EP4. This concentration of ONO-AE3-208 reached the Ki of EP3 and could also antagonize EP3. The EP3 signal inhibits adenylate cyclase, and thus the antagonism of EP3 increases intracellular cAMP concentrations (15). However, the suppression level of cAMP was proportional to the ONO-AE3-208 concentrations, suggesting

that antagonistic effect against EP3 might be slight. The PSA expression of LNCaP-EP4 cells without androgen was also suppressed by the same concentrations of ONO-AE3-208 (Fig. 4A).

We then examined the *in vivo* antitumor effect of ONO-AE3-208. I.p. injection of ONO-AE3-208 (10 mg/kg; once a day) suppressed the castration-resistant growth of LNCaP-EP4 xenograft tumors (Fig. 4B). The serum PSA values of LNCaP-EP4 xenograft mice were also significantly decreased (median PSA at sacrifice: 5.7 and 3.7 ng/mL in controls and AE3-208, respectively, $P < 0.05$). The mean body weight of mice in the control and AE3-208 groups were almost the same, and no mice died during the treatment, indicating that ONO-AE3-208 was well tolerated at the concentrations used. The same dose of ONO-AE3-208 also suppressed the castration-resistant growth of KUCaP-2 tumors (Fig. 4C). The PSA production of KUCaP-2 tumors was significantly decreased (median PSA at sacrifice: 17.4 and 9.4 ng/mL in controls and AE3-208, respectively, $P < 0.05$). There were no significant differences in EP4 expression between the tumors of the control and AE3-208 groups (data not shown), indicating that ONO-AE3-208 antagonized EP4 without suppressing the receptor expression. In summary, EP4 antagonism with ONO-AE3-208 might be an effective and tolerable treatment modality for CRPC, in which EP4 overexpression induced castration-resistant progression (Fig. 4D).

Discussion

As CRPC is a heterogeneous group of diseases (16), many experimental models are required to elucidate the mechanisms for castration resistance. However, limited tissue availability for molecular studies and few available human prostate cancer cell lines with both AR- and androgen-dependent states have restricted prostate cancer research. Xenografts are models in which human tissue is transplanted into an immunodeficient mouse. In this way, human prostate cancer can be propagated *in vivo* for long periods to allow the study of tumor progression under different experimental hormonal conditions and to support the testing of novel therapies. Before 1993, only one prostate cancer xenograft, LNCaP

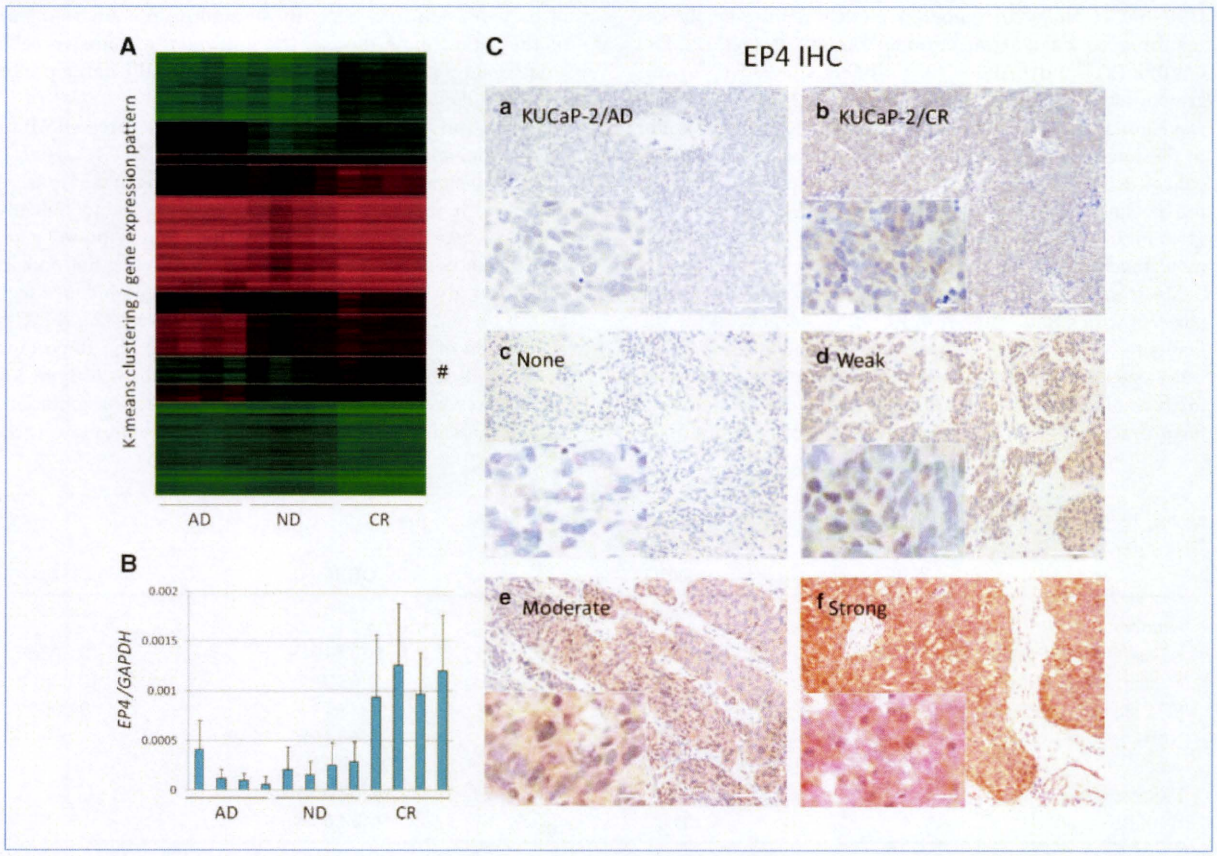

Figure 2. EP4 expression was upregulated during the castration-resistant progression of KUCaP-2. A, the *k*-means clustering of the DNA microarray data for AD, ND, and CR stage tumors of KUCaP-2. The *EP4* is in the cluster indicated with #. B, expression levels of *EP4* validated by real-time PCR analysis. C, the EP4 immunohistochemistry of AD stage (a) and CR stage (b) tumors of KUCaP-2. The staining intensity of EP4 in clinical samples of prostate cancer patients graded as none (c), weak (d), moderate (e) and strong (f). Scale bars, 50 μm, inset 5 μm.

Table 1. Significantly upregulated genes at CR compared with AD and ND stages (10 highest CR/ND ratio)

Gene name (symbol)	CR/AD		CR/ND	
	Ratio	*P*	Ratio	*P*
Prostaglandin E receptor EP4 subtype (EP4)	15.7	0.01048	15.7	0.02903
Lumican (LUM)	23.6	0.00110	14.2	0.01095
Natriuretic peptide receptor C (NPRC)	2.3	0.19044	8.1	0.04921
N-methyl-D-aspartate 3A (GRIN3A)	9.1	0.00006	7.4	0.00029
Neuroligin 1 (NLGN1)	7.9	0.01844	6.1	0.04429
Coiled-coil domain containing 68 (CCDC68)	7.4	0.00013	4.4	0.00460
Tissue factor pathway inhibitor (TFPI)	4.1	0.04105	4.2	0.04678
Secretoglobin, family 1D, member 2 (LIPB)	8.2	0.01950	3.8	0.06641
Nudix-type motif 11 (UNDT11)	4.0	0.00444	3.7	0.01913
Eukaryotic translation initiation factor 1A Y-linked (EIF1AY)	2.6	0.07360	3.3	0.04354

(17), had been reported to be androgen dependent. LNCaP tumors shrink slightly after castration, usually with less than a 10% reduction in volume, and regrow less than 5 weeks after castration. Thereafter, several androgen-dependent xenografts have also been established. The LAPC-4 (18), LuCaP-23 (19), and PC346P (20) xenograft models reportedly show a response to castration similar to that of LNCaP. The CWR22 (21) and LAPC-9 (22) models showed recurrent growth after androgen ablation after 3 to 6 months, which was similar to our established xenograft, KUCaP-2. Similar to these models that mimic the clinical behavior of prostate cancer, KUCaP-2 may provide an excellent system to study the mechanisms associated with the castration-resistant progression of prostate cancer and help us develop novel treatment modalities against CRPC.

Most androgen-dependent xenografts were derived from patients with CRPC, as seen in KUCaP-2, because of the difficulty to obtain enough samples from patients with HNPC. It was suggested that prostate cancer contain a heterogeneous mixture of cells that vary in their dependence on androgen for growth and survival, and that treatment with androgen ablation therapy provides selective pressure and alters the relative concentration of these cells, thereby leading to the outgrowth of CRPC (22). These tumors presumably contain a mixture of growth-arrested, androgen-responsive tumor cells in addition to androgen-independent cells at the time of implantation into mice. In the androgenic environment of the intact male mouse, the androgen-responsive cells would gain a growth advantage and eventually develop into androgen-dependent xenografts.

The castration-resistant KUCaP-2 tumors expressed AR in their nuclei and produced PSA, suggesting that AR was activated with significantly low circulating androgen and is associated with the castration-resistant progression. Recent findings suggest that AR is an important transcription factor that mediates survival and proliferation signaling not only in HNPC but also in CRPC (23, 24). The androgen-independent activation of AR is mediated by several pathways (25, 26). The acquisition of mutations in *AR* is likely to be an important pathway (3, 27). However, KUCaP-2 harbors wild-type AR and progresses to castration resistance without AR mutation. Another possible pathway is its hypersensitivity to low levels

Table 2. Patient characteristics and EP4 staining grade in HNPC and CRPC

	HNPC	CRPC	*P*
Number	27	31	
Median serum PSA (ng/mL)	7.9 (3.8–31.3)	15.5 (0.5–949)	0.0066*
Median Gleason sum	7 (3–9)	9 (6–10)	0.0001*
EP4 staining grade†			0.0001‡
None	10 (37.0%)	5 (16.1%)	
Weak	17 (63.0%)	9 (29.1%)	
Moderate	0 (0%)	10 (32.2%)	
Strong	0 (0%)	7 (22.6%)	

*Mann-Whitney *U* test.
†The grading was determined on the intensity of staining for at least 20% of the cancer cells.
‡χ^2 test between HNPC and CRPC.

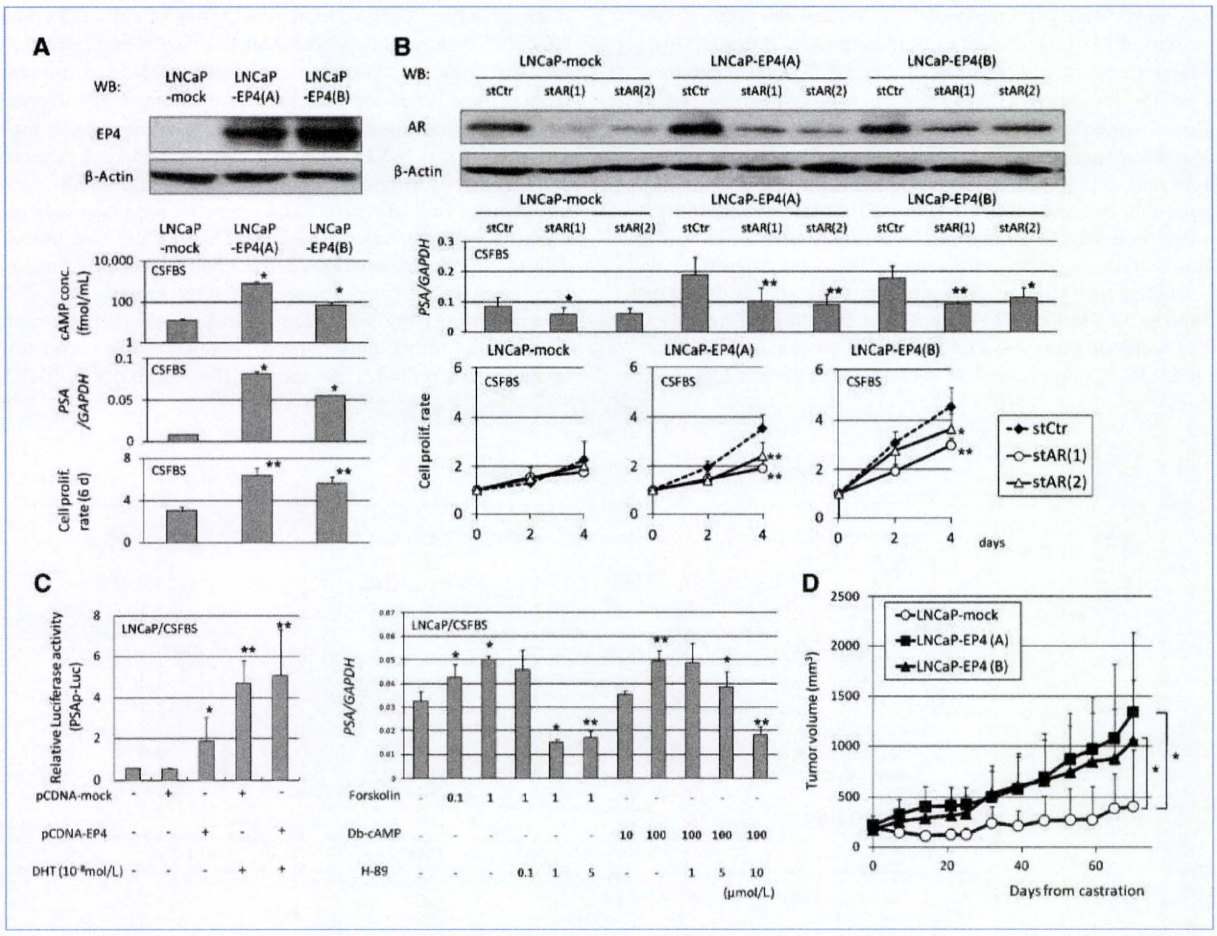

Figure 3. Overexpression of EP4 with cAMP-PKA signal activation promoted the castration-resistant progression of LNCaP cells through AR activation. A, EP4 protein expression detected with Western blotting in LNCaP-EP4(A) and LNCaP-EP4(B) compared with LNCaP-mock (top), intracellular cAMP concentrations, *PSA* expression, and cell proliferation ratio versus day 0 in androgen-depleted conditions (CSFBS) for 6 d (bottom). *, $P < 0.05$; **, $P < 0.005$ versus LNCaP-mock. B, AR expression attenuated using a stealth RNAi system detected with Western blotting (top), *PSA* expression levels on day 4 (middle), and cell proliferation ratio on days 2 and 4 versus day 0 (bottom) in CSFBS. *, $P < 0.05$; **, $P < 0.005$ versus LNCaP-mock. C, relative luciferase activities of PSAp-Luc in LNCaP cells with transfection of pcDNA3.1-mock and pcDNA3.1-EP4 in CSFBS and 5α-dihydrotestosterone (DHT) stimulation, respectively. *, $P < 0.05$; **, $P < 0.005$ versus control (left). PSA expression of LNCaP cells in CSFBS for 6 d under the administration of forskolin, dbcAMP, and H-89. *, $P < 0.05$; **, $P < 0.005$ versus preadministration (right). D, the sequential changes in xenograft tumor volume after the castration of mice (1×10^7 cells, $n = 5$ each). *, $P < 0.05$.

of androgens, induced by increased expression of the AR itself (10). In KUCaP-2, the *AR* mRNA expression slightly increased from the AD to ND and CR stages. However, the AR protein expression levels decreased at the ND stage and recovered at the CR stage to the same level as the AD stage both in the AR immunohistochemistry (Fig. 1D) and Western blotting (data not shown) analysis. One possible explanation for this discrepancy is that the AR protein might be degraded without androgen at ND stage and stabilized at the CR stage (28, 29). These results indicated that the upregulation of *AR* might merely be an adaptation of tumor cells to the condition of low androgen stimulation and not an essential indicator of castration-resistant progression. EP4 upregulation was observed during castration-resistant progression in KUCaP-2. EP4 expression was higher in clinical CRPC than in HNPC. The xenograft of EP4-overexpressing LNCaP cells developed castration resistance through AR activation. These results revealed that EP4 upregulation might lead to AR activation, resulting in the castration-resistant progression of prostate cancer. It was reported that the activation of a membrane-localized G protein-coupled receptor induced nuclear partition and activation of AR through the accumulation of intracellular cAMP and PKA activation (30). As EP4 is a G protein-coupled receptor, our data showing that EP4-cAMP-PKA axis activates AR are consistent to the report.

EP4 is one of the prostaglandin E2 (PGE2) receptors. PGE2, the product of cyclooxygenase-2 (COX-2) conversion of plasma membrane phospholipids, is the most common prostanoid and is associated with inflammatory disease (14) and cancer (31, 32). It was suggested that inflammation plays a

role in prostate carcinogenesis (33, 34) and the regular consumption of non-steroidal anti-inflammatory drugs (NSAID) may reduce the risk of prostate cancer (35–37). Therefore, NSAIDs, including COX-2 inhibitors, have been tested in the treatment (38) and prevention (39) of prostate cancer. However, these approaches have met with limited success (40) and, sometimes, severe cardiovascular side effects (41), probably because COX-2 produces multiple products with pleiotropic effects in addition to PGE2. Therefore, targeting downstream signaling pathways of PGE2 may represent an attractive new strategy. There are four subtypes of PGE2 receptors, EP1 to EP4. The intracellular signaling differs among the receptor subtypes; EP1 is coupled to calcium mobilization, EP3 inhibits adenylate cyclase, and EP2 and EP4 stimulate adenylate cyclase in various types of cells (42). The effects of PGE2 are dependent on the ligand concentration and the target cell receptor expression (32). Experimental studies have suggested that increased EP2 and EP4 expression is important during colorectal and prostate cancer progression (43, 44). In KUCaP-2, EP2 expression did not increase significantly during castration-resistant progression (data not shown), indicating that EP4 might be more strongly associated with castration resistance than EP2 in this model. To examine the association of PGE2 and cancer progression, the serum PGE2 concentrations of mice bearing KUCaP-2 were examined by PGE2 Express EIA kit (500141; Cayman Chemical). Unfortunately, reproducible results could not be obtained, probably because of the instability of PGE2.

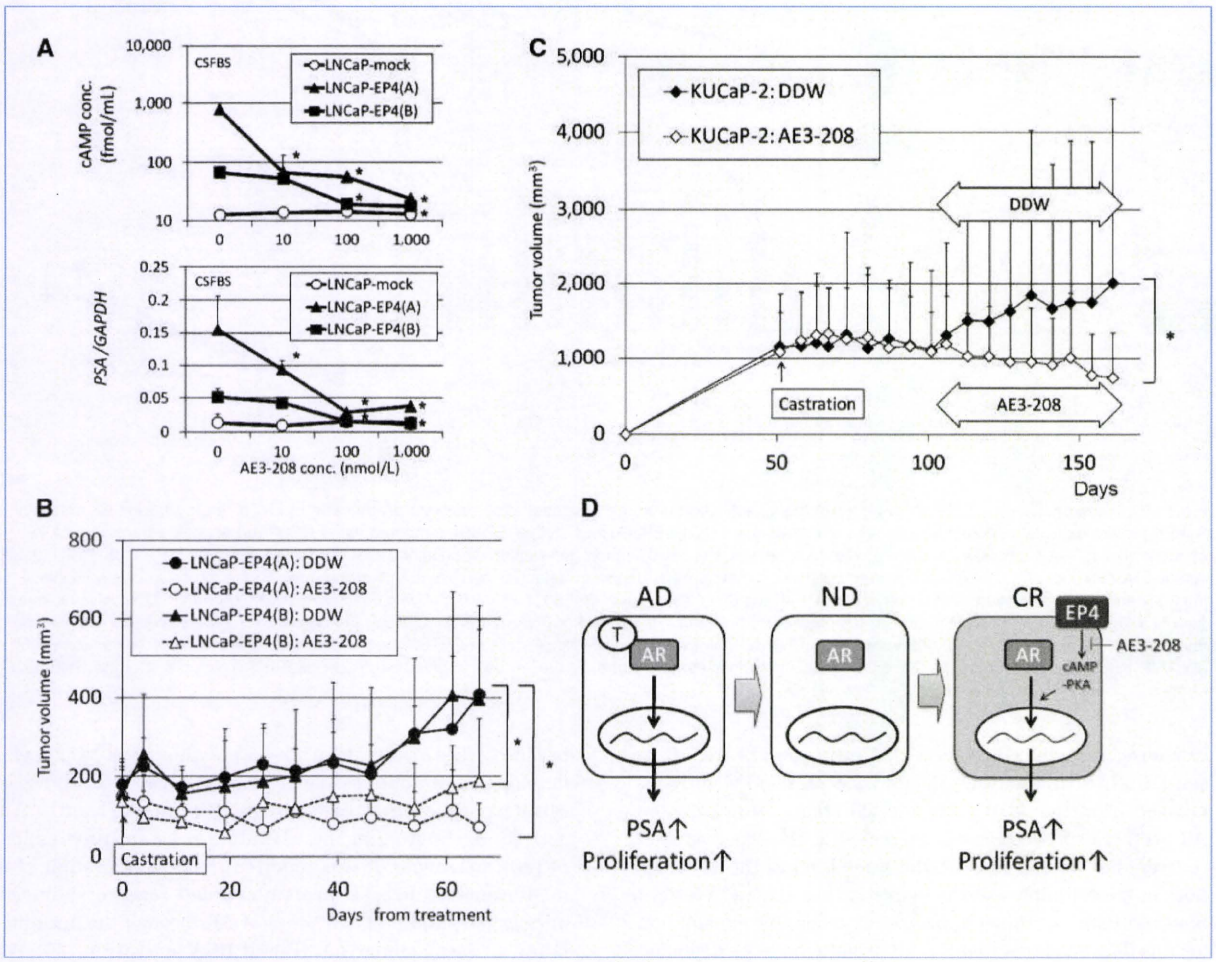

Figure 4. Castration-resistant progression of LNCaP-EP4 and KUCaP-2 was suppressed by ONO-AE3-208 treatment. A, the cAMP concentration (top) and *PSA* expression (bottom) of LNCaP-mock, LNCaP-EP4(A), and LNCaP-EP4(B) under the *in vitro* administration of ONO-AE3-208 in CSFBS. *, $P < 0.05$ versus LNCaP-mock. B, the sequential changes in LNCaP-EP4(A) and LNCaP-EP4(B) xenograft tumors treated with i.p. injection of 200 μL/d distilled water (DDW) and 10 mg/kg/d ONO-AE3-208 (AE3-208) started soon after the castration of mice and continued for 70 d (0.5×10^7 cells, $n = 5$ each). *, $P < 0.05$. C, the sequential changes in KUCaP-2 tumors treated with the same volume of DDW and AE3-208 solution started 50 d after castration and continued for 60 d ($n = 5$ each). *, $P < 0.05$. D, schematic representation of the relationship between EP4 overexpression and castration resistance. After castration, the upregulated EP4 induces activation of the AR without androgen and promotes castration-resistant cell proliferation and PSA production, which is suppressed by ONO-AE3-208 administration. T, androgen.

Therefore, it might be difficult to examine the serum PGE2 concentrations in clinical samples. The secreted PGE2 concentrations in LNCaP-EP4 cells were higher than in LNCaP-mock cells [20.3 ± 15.4, 48.7 ± 4.9, and 44.7 ± 11.5 pg/mL in LNCaP-mock, LNCaP-EP4(A), and LNCaP-EP4(B), respectively]. However, the administration of PGE2 into LNCaP-EP4 could not induce cell proliferation and PSA production. To elucidate the association of PGE2 and cancer progression needs further examinations.

The cell proliferation of LNCaP-EP4 was significantly higher than that of LNCaP-mock under androgen-depleted medium but not under normal medium (data not shown), indicating that EP4 overexpression enhanced androgen-independent but not androgen-dependent proliferation of LNCaP cells *in vitro*. However, the *in vivo* tumor growth of LNCaP-EP4 was significantly higher than that of LNCaP-mock in intact mice (193 ± 76 and 121 ± 46 mm^3 on day 30, respectively, $P = 0.003$). Moreover, the xenograft tumor take-up rate of LNCaP-EP4 was higher than that of LNCaP-mock (~100% and 60%, respectively). It was reported that PGE2 regulated angiogenesis in PC3 cells through EP2 and EP4 (44). Therefore, it was suggested that EP4 overexpression might increase cell proliferation of LNCaP cells *in vivo* through angiogenesis. The PSA expression of LNCaP-EP4 was significantly higher than that of LNCaP-mock under androgen-depleted medium. Although EP4 expression was higher in LNCaP-EP4(B) than in LNCaP-EP4(A), the intracellular cAMP concentration and PSA expression levels were higher in LNCaP-EP4(A) than in LNCaP-EP4(B). To investigate the reasons for the discrepancy, we performed transient transfection analyses with several different amounts of pcDNA3.1-EP4. The PSA expression levels were correlated with EP4 expression levels in LNCaP cells transiently transfected with the EP4 expression vector, suggesting that the reasons for this discrepancy might be clonal variations of LNCaP-EP4 (data not shown). The expression of TMPRSS2, one of other AR-regulated genes (45), was also increased with EP4 overexpression and decreased by the attenuation of AR (data not shown). These results indicated that EP4 may increase PSA expression partly in an AR-dependent manner; however, we do not exclude possibilities that EP4 increases PSA and TMPRSS2 expressions through an AR-independent manner. Analysis of these mechanisms needs further investigations.

It was suggested that the EP4-cAMP-PKA axis can activate the β-catenin/TCF signaling pathway, leading to cancer progression (46), and that the EP4-specific antagonist, ONO-AE3-208, inhibits the progression of EP4-expressing colorectal cancer (47, 48). The present study is the first report showing that ONO-AE3-208 reduces the castration-resistant progression of prostate cancer cells induced by EP4 overexpression. ONO-AE3-208 did not suppress the proliferation of KUCaP-2 in intact mice (data not shown), suggesting that EP4 antagonism might have no antitumor effect against HNPC. DU145 and PC3 are AR-negative prostate cancer cells with high EP4 expression. The *in vitro* administration of 100 nmol/L ONO-AE3-208 decreased intracellular cAMP concentrations of these cells. However, it did not suppress their cell proliferation *in vitro* and *in vivo* (data not shown). It was suggested that the EP4-cAMP-PKA axis might not be associated with their cell proliferation.

In conclusion, we found that EP4 overexpression is one of the mechanisms responsible for progression to CRPC using a novel xenograft model KUCaP-2. The administration of EP4 antagonist *in vivo* suppressed the castration-resistant progression of KUCaP-2, indicating that EP4 may be a potential target for the treatment of CRPC.

Disclosure of Potential Conflicts of Interest

No potential conflicts of interest were disclosed.

Acknowledgments

We thank Tomoko Kobayashi and Megumi Kishida for their valuable technical assistance.

Grant Support

Grants-in-aid for scientific research from the Ministry of Education, Culture, Sports, Science and Technology of Japan.

The costs of publication of this article were defrayed in part by the payment of page charges. This article must therefore be hereby marked *advertisement* in accordance with 18 U.S.C. Section 1734 solely to indicate this fact.

Received 8/11/09; revised 11/30/09; accepted 12/2/09; published OnlineFirst 2/9/10.

References

1. Gronberg H. Prostate cancer epidemiology. Lancet 2003;361:859–64.
2. Petrylak DP, Tangen CM, Hussain MH, et al. Docetaxel and estramustine compared with mitoxantrone and prednisone for advanced refractory prostate cancer. N Engl J Med 2004;351:1513–20.
3. Yoshida T, Kinoshita H, Segawa T, et al. Antiandrogen bicalutamide promotes tumor growth in a novel androgen-dependent prostate cancer xenograft model derived from a bicalutamide-treated patient. Cancer Res 2005;65:9611–6.
4. Terada N, Shimizu Y, Yoshida T, et al. Antiandrogen withdrawal syndrome and alternative antiandrogen therapy associated with the W741C mutant androgen receptor in a novel prostate cancer xenograft. Prostate. Epub 2009.
5. Kabashima K, Sakata D, Nagamachi M, Miyachi Y, Inaba K, Narumiya S. Prostaglandin E2-4 signaling initiates skin immune responses by promoting migration and maturation of Langerhans cells. Nat Med 2003;9:744–9.
6. Bastien L, Sawyer N, Grygorczyk R, Metters KM, Adam M. Cloning, functional expression, and characterization of the human prostaglandin E2 receptor EP2 subtype. J Biol Chem 1994;269:11873–7.
7. Inoue T, Yoshida T, Shimizu Y, et al. Requirement of androgen-dependent activation of protein kinase Cζ for androgen-dependent cell proliferation in LNCaP cells and its roles in transition to androgen-independent cells. Mol Endocrinol 2006;20:3053–69.
8. Inoue T, Segawa T, Shiraishi T, et al. Androgen receptor, Ki67, and p53 expression in radical prostatectomy specimens predict treatment failure in Japanese population. Urology 2005;66:332–7.
9. Shimizu Y, Segawa T, Inoue T, et al. Increased Akt and phosphorylated Akt expression are associated with malignant biological features of prostate cancer in Japanese men. BJU Int 2007;100:685–90.

10. Chen CD, Welsbie DS, Tran C, et al. Molecular determinants of resistance to antiandrogen therapy. Nat Med 2004;10:33–9.
11. Chen Y, Hughes-Fulford M. Prostaglandin E2 and the protein kinase A pathway mediate arachidonic acid induction of c-fos in human prostate cancer cells. Br J Cancer 2000;82:2000–6.
12. Liu XH, Kirschenbaum A, Lu M, et al. Prostaglandin E2 induces hypoxia-inducible factor-1α stabilization and nuclear localization in a human prostate cancer cell line. J Biol Chem 2002;277:50081–6.
13. Wang X, Klein RD. Prostaglandin E2 induces vascular endothelial growth factor secretion in prostate cancer cells through EP2 receptor-mediated cAMP pathway. Mol Carcinog 2007;46:912–23.
14. Matsuoka T, Narumiya S. The roles of prostanoids in infection and sickness behaviors. J Infect Chemother 2008;14:270–8.
15. Yang L, Huang Y, Porta R, et al. Host and direct antitumor effects and profound reduction in tumor metastasis with selective EP4 receptor antagonism. Cancer Res 2006;66:9665–72.
16. Shah RB, Mehra R, Chinnaiyan AM, et al. Androgen-independent prostate cancer is a heterogeneous group of diseases: lessons from a rapid autopsy program. Cancer Res 2004;64:9209–16.
17. Gleave ME, Hsieh JT, Wu HC, von Eschenbach AC, Chung LW. Serum prostate specific antigen levels in mice bearing human prostate LNCaP tumors are determined by tumor volume and endocrine and growth factors. Cancer Res 1992;52:1598–605.
18. Klein KA, Reiter RE, Redula J, et al. Progression of metastatic human prostate cancer to androgen independence in immunodeficient SCID mice. Nat Med 1997;3:402–8.
19. Ellis WJ, Vessella RL, Buhler KR, et al. Characterization of a novel androgen-sensitive, prostate-specific antigen-producing prostatic carcinoma xenograft: LuCaP 23. Clin Cancer Res 1996;2:1039–48.
20. Marques RB, van Weerden WM, Erkens-Schulze S, et al. The human PC346 xenograft and cell line panel: a model system for prostate cancer progression. Eur Urol 2006;49:245–57.
21. Nagabhushan M, Miller CM, Pretlow TP, et al. CWR22: the first human prostate cancer xenograft with strongly androgen-dependent and relapsed strains both *in vivo* and in soft agar. Cancer Res 1996;56:3042–6.
22. Craft N, Chhor C, Tran C, et al. Evidence for clonal outgrowth of androgen-independent prostate cancer cells from androgen-dependent tumors through a two-step process. Cancer Res 1999; 59:5030–6.
23. Inoue T, Kobayashi T, Terada N, et al. Roles of androgen-dependent and -independent activation of signal transduction pathways for cell proliferation of prostate cancer cells. Expert Rev Endocrinol Metab 2007;2:689–704.
24. Wang Q, Li W, Zhang Y, et al. Androgen receptor regulates a distinct transcription program in androgen-independent prostate cancer. Cell 2009;138:245–56.
25. Nelson WG, De Marzo AM, Isaacs WB. Prostate Cancer. N Engl J Med 2003;349:366–81.
26. Feldman BJ, Feldman D. The development of androgen-independent prostate cancer. Nat Rev Cancer 2001;1:34–45.
27. Taplin ME, Balk SP. Androgen receptor: a key molecule in the progression of prostate cancer to hormone independence. J Cell Biochem 2004;91:483–90.
28. Gregory CW, Johnson RT, Jr., Mohler JL, French FS, Wilson EM. Androgen receptor stabilization in recurrent prostate cancer is associated with hypersensitivity to low androgen. Cancer Res 2001;61: 2892–8.
29. Lee DK, Chang C. Endocrine mechanisms of disease: expression and degradation of androgen receptor: mechanism and clinical implication. J Clin Endocrinol Metab 2003;88:4043–54.
30. Kasbohm EA, Guo R, Yowell CW, et al. Androgen receptor activation by G(s) signaling in prostate cancer cells. J Biol Chem 2005;280: 11583–9.
31. Oshima M, Dinchuk JE, Kargman SL, et al. Suppression of intestinal polyposis in Apc δ716 knockout mice by inhibition of cyclooxygenase 2 (COX-2). Cell 1996;87:803–9.
32. Hull MA, Ko SC, Hawcroft G. Prostaglandin EP receptors: targets for treatment and prevention of colorectal cancer? Mol Cancer Ther 2004;3:1031–9.
33. Platz EA, De Marzo AM. Epidemiology of inflammation and prostate cancer. J Urol 2004;171:S36–40.
34. De Marzo AM, Platz EA, Sutcliffe S, et al. Inflammation in prostate carcinogenesis. Nat Rev Cancer 2007;7:256–69.
35. Mahmud S, Franco E, Aprikian A. Prostate cancer and use of nonsteroidal anti-inflammatory drugs: systematic review and meta-analysis. Br J Cancer 2004;90:93–9.
36. Gupta S, Adhami VM, Subbarayan M, et al. Suppression of prostate carcinogenesis by dietary supplementation of celecoxib in transgenic adenocarcinoma of the mouse prostate model. Cancer Res 2004; 64:3334–43.
37. Singer EA, Palapattu GS, van Wijngaarden E. Prostate-specific antigen levels in relation to consumption of nonsteroidal anti-inflammatory drugs and acetaminophen: results from the 2001-2002 National Health and Nutrition Examination Survey. Cancer 2008;113:2053–7.
38. Smith MR, Manola J, Kaufman DS, Oh WK, Bubley GJ, Kantoff PW. Celecoxib versus placebo for men with prostate cancer and a rising serum prostate-specific antigen after radical prostatectomy and/or radiation therapy. J Clin Oncol 2006;24:2723–8.
39. Lieberman R. Chemoprevention of prostate cancer: current status and future directions. Cancer Metastasis Rev 2002;21:297–309.
40. Csiki I, Morrow JD, Sandler A, et al. Targeting cyclooxygenase-2 in recurrent non-small cell lung cancer: a phase II trial of celecoxib and docetaxel. Clin Cancer Res 2005;11:6634–40.
41. Ray WA, Stein CM, Daugherty JR, Hall K, Arbogast PG, Griffin MR. COX-2 selective non-steroidal anti-inflammatory drugs and risk of serious coronary heart disease. Lancet 2002;360:1071–3.
42. Sugimoto Y, Narumiya S. Prostaglandin E receptors. J Biol Chem 2007;282:11613–7.
43. Sonoshita M, Takaku K, Sasaki N, et al. Acceleration of intestinal polyposis through prostaglandin receptor EP2 in Apc(Δ716) knockout mice. Nat Med 2001;7:1048–51.
44. Jain S, Chakraborty G, Raja R, Kale S, Kundu GC. Prostaglandin E2 regulates tumor angiogenesis in prostate cancer. Cancer Res 2008; 68:7750–9.
45. Iljin K, Wolf M, Edgren H, et al. TMPRSS2 fusions with oncogenic ETS factors in prostate cancer involve unbalanced genomic rearrangements and are associated with HDAC1 and epigenetic reprogramming. Cancer Res 2006;66:10242–6.
46. Chell S, Kaidi A, Williams AC, Paraskeva C. Mediators of PGE2 synthesis and signalling downstream of COX-2 represent potential targets for the prevention/treatment of colorectal cancer. Biochim Biophys Acta 2006;1766:104–19.
47. Mutoh M, Watanabe K, Kitamura T, et al. Involvement of prostaglandin E receptor subtype EP(4) in colon carcinogenesis. Cancer Res 2002;62:28–32.
48. Chell SD, Witherden IR, Dobson RR, et al. Increased EP4 receptor expression in colorectal cancer progression promotes cell growth and anchorage independence. Cancer Res 2006;66:3106–13.

Bioorganic & Medicinal Chemistry Letters 20 (2010) 1718–1720

Contents lists available at ScienceDirect

Bioorganic & Medicinal Chemistry Letters

journal homepage: www.elsevier.com/locate/bmcl

Design, synthesis, evaluation and QSAR analysis of N^1-substituted norcymserine derivatives as selective butyrylcholinesterase inhibitors

Jun Takahashi [a], Ichiro Hijikuro [e], Takeshi Kihara [a], Modachur G. Murugesh [e], Shinichiro Fuse [d], Ryo Kunimoto [c], Yoshinori Tsumura [b], Akinori Akaike [b], Tetsuhiro Niidome [a], Yasushi Okuno [c], Takashi Takahashi [d], Hachiro Sugimoto [a,*]

[a] Department of Neuroscience for Drug Discovery, Graduate School of Pharmaceutical Sciences, Kyoto University, 46-29 Yoshida-Shimoadachi-cho, Sakyo-ku, Kyoto 606-8501, Japan
[b] Department of Pharmacology, Graduate School of Pharmaceutical Sciences, Kyoto University, 46-29 Yoshida-Shimoadachi-cho, Sakyo-ku, Kyoto 606-8501, Japan
[c] Department of Systems Bioscience for Drug Discovery, Graduate School of Pharmaceutical Sciences, Kyoto University, 46-29 Yoshida-Shimoadachi-cho, Sakyo-ku, Kyoto 606-8501, Japan
[d] Department of Applied Chemistry, Graduate School of Science and Engineering, Tokyo Institute of Technology, 2-12-1 Ookayama, Meguro, Tokyo 152-8552, Japan
[e] Department of Development, ChemGenesis Incorporated, 4-10-1 Nihonbashi-Honcho, Chuo-ku, Tokyo 103-0023, Japan

ARTICLE INFO

Article history:
Received 26 November 2009
Revised 7 January 2010
Accepted 8 January 2010
Available online 20 January 2010

Keywords:
Acetylcolinesterase
Butyrylcholinesterase
Alzheimer's disease
Carbamate

ABSTRACT

We synthesized a series of N^1-substituted norcymserine derivatives **7a–p** and evaluated their anti-cholinesterase activities. In vitro evaluation showed that the pyridinylethyl derivatives **7m–o** and the piperidinylethyl derivative **7p** improved the anti-butyrylcholinesterase activity by approximately threefold compared to N^1-phenethylnorcymserine (PEC, **2**). A quantitative structure-activity relationship (QSAR) study indicated that log*S* might be a key feature of the improved compounds.

Alzheimer's disease (AD) is one of the primary neurodegenerative diseases that develops in the elderly, and its prevalence is expected to increase substantially in the future.[1] While AD is definitively characterized by its pathological hallmarks, such as senile plaques and neurofibrillary tangles, in the postmortem brain, AD is diagnosed by the progressive cognitive impairment observed in living patients. Since the decline of cholinergic neurotransmission is responsible for cognitive dysfunction, considerable effort has been devoted to developing effective cholinesterase inhibitors (ChEIs).

Acetylcholinesterase (AChE) is the main cholinesterase (ChE) in the brain, and hence most works aimed at developing ChEIs have targeted AChE. To date, some AChE inhibitors have been clinically approved, and use of these inhibitors has been successful in the treatment of AD. However, in the AD brain, cholinergic neurons are lost along with the progression of the disease and AChE is also reduced.[2]

Vertebrates have another acetylcholine (ACh) hydrolase known as butyrylcholinesterase (BuChE). In contrast to AChE, BuChE is mainly derived from glia in the brain.[3] BuChE is therefore not reduced, and its contribution in degrading ACh is thought to be increased in the AD brain.[2] Interestingly, it has been reported that selective BuChE inhibitors (BuChEIs) increase the brain ACh,[4] and BuChE knockout mice and silent mutants in humans showed no physiological disadvantage,[5,6] inspiring the hypothesis that BuChE may be a promising target for developing anti-AD drugs with no adverse effect.

Physostigmine (**1**), an alkaloid isolated from the Calabar bean, the seed of *Physostigma venenosum*, is the most classical ChEI, and still used in the treatment of glaucoma. Although many mechanistic studies have been carried out, clarification of three-dimensional structures of AChE[7] and BuChE[8] have enabled us to investigate the detailed enzyme-inhibitor interaction. For instance, regarding the N^1-position of the physostigmine derivatives, the bulkiness of substituents at this position affects the enantioselectivity at **3a**, and the phenethyl group renders the compounds more selective for BuChE than their corresponding N^1-H and N^1-Me analogs.[9–11] It has also been reported that N^1-phenethylnorcymserine (PEC, **2**) exhibits the property of a potent and selective BuChEI.[12]

Although these findings were intriguing, these studies did not investigate a large variety of substituents and, overall, they were limited to relatively simple compounds. Hence, previous report studying the quantitative structure–activity relationship (QSAR) has pointed out that large polar and large hydrophobic substituents would have to be synthesized and tested.[13] An investigation

* Corresponding author. Tel.: +81 75 753 9270; fax: +81 75 753 9269.
E-mail address: hsugimot@pharm.kyoto-u.ac.jp (H. Sugimoto).

0960-894X/$ - see front matter © 2010 Elsevier Ltd. All rights reserved.
doi:10.1016/j.bmcl.2010.01.057

using more diverse derivatives may increase our understanding and help improve the development of better compounds. In light of this, we investigated the structure-activity relationship of the N^1 moiety of norcymserine derivatives **1**, **2**, **3** and **7a–p** in this report. Furthermore, for a detailed understanding, we carried out the QSAR study. For all compounds, the carbamate moiety was fixed in the shape of 4-isopropylphenylcarbamate, because this structural arrangement increases the potency and the selectivity for BuChE.[12]

PEC (**2**) and cymserine (**3**) were prepared according to procedures described previously.[9,14] A series of N^1-substituted norcymserine derivatives **7a–p** were synthesized via intermediates **5a–p** as indicated in Scheme 1. Ammonium iodide (**4**), prepared from physostigmine (**1**) using four steps,[14] was treated with different R–NH_2 compounds (**b**, **d–l** and **o**, Scheme 1),[9,11,15] followed by demethylation with BBr_3[9–12,16] to generate N^1-substituted noreserolines (**5b**, **5d–l** and **5o**). Alternatively, the intermediate **5** was prepared using only one step in a convenient one-pot procedure.[17] Physostigmine (**1**) was reacted with KOH and MeI in DMSO at room temperature for 1 h, before the addition of different R–NH_2 compounds (**a**, **c**, **m**, **n** and **p**, Scheme 1). After the reaction mixtures were stirred at 120 °C for 3 h, N^1-substituted noreserolines **5a**, **5c**, **5m**, **5n** and **5p** were obtained at 10–21% yield, accompanied by the corresponding methyl ethers **6a**, **6c**, **6m**, **6n** and **6p** at 0–10% yield, respectively. Finally, the N^1-substituted norcymserine derivatives **7a–p** were prepared from **5a–p** using previously reported methods.[9–12,16]

Anti-ChE activities were measured using a modified Ellman's colorimetric method.[18] Briefly, we used the extracts from mice brain and mice serum as sources of AChE and BuChE, respectively, and all compounds were preincubated with enzymes for 1 h at 37 °C before adding acetylthiocholine or butyrylthiocholine in combination with the coloring reagent 5,5′-dithiobis-(2-nitrobenzoic acid).

The IC_{50} values for AChE and BuChE are summarized in Table 1. We first assessed whether the length of the alkyl chain had an influence on anti-BuChE activity, and we found that the activity did not differ between the N^1-benzyl, -phenetyl, -phenylpropyl and -phenylbutyl derivatives (**2** and **7a–c**). Since the length of the alkyl chain did not influence the activity, we subsequently investigated the effects of various substituents on the phenethyl group. Neither electron-donating nor electron-withdrawing group at the 4-position of the phenyl group influenced the activity (**7d–f**). On the other hand, bulky substituent at the same position was shown to reduce the activity (**7g**). Disubstituents at the 2 and 4-position of the phenyl group also lowered the potency of the compounds (**7h and 7i**). The increased bulkiness of the alkyl chain of the phenethyl group also decreased the anti-BuChE activity (**7j–l**). Most physostigmine derivatives reported previously did not include a heteroatom in its N^1-substituents. Therefore, we also examined the effects of the substitution of heterocycles for the phenyl ring of the phenethyl group. Substitution of pyridine for the phenyl group increased the anti-BuChE activity by approximately threefold regardless of the position of the nitrogen on the pyridine, and the 1-piperidinylethyl group substitution exhibited a similar activity (**7m–p**).

The QSAR study probing the N^1-position of physostigmine derivatives has ever been conducted using a small dataset, and was used to evaluate for the anti-AChE activity.[19] Therefore, in order to rationalize the observed anti-BuChE activities, we carried out the QSAR study.

For the QSAR study dataset, the structures of all compounds excluding physostigmine, and their corresponding pIC_{50} values for BuChE were used. The chemical structures were drawn using CHEMDRAW Std 7.0 (Chembridge Soft. com) and the database was exported as an sdf file and imported into the MOE software (version 2008.10, Chemical Computing Group). Notably, the calculations were performed using the appropriately ionized form. The QSAR model generation was done using AutoQSAR packaged in MOE, and the QSAR models were constructed based on the partial least square method using 327 descriptors built in MOE. The equation we obtained was shown below:

$$pIC_{50} = 0.452(0.044)\log S - 0.051(0.009)\text{weinerPol} + 0.010(0.002)\text{PEOE\_VSA-0} + 0.327(0.049)\text{opr\_violation} + 10.556(0.413)$$

$$n = 18, \quad RMSE = 0.080, \quad R^2 = 0.980,$$

cross-validated $RMSE = 0.187$,

$$Q^2 = 0.909, \quad S = 0.094, \quad F_{4,13} = 160.2$$

In the QSAR equation, log*S* is the log of the aqueous solubility, weinerPol is the Wiener polarity number,[20] PEOE_VSA-0 is the sum of the van der Waals surface area of atoms where the atomic partial charges are ranging from −0,05 to 0, opr_violation is the number of violations of Oprea's lead-like test,[21] *n* is the number of compounds, *RMSE* is the root mean square error, R^2 is the goodness

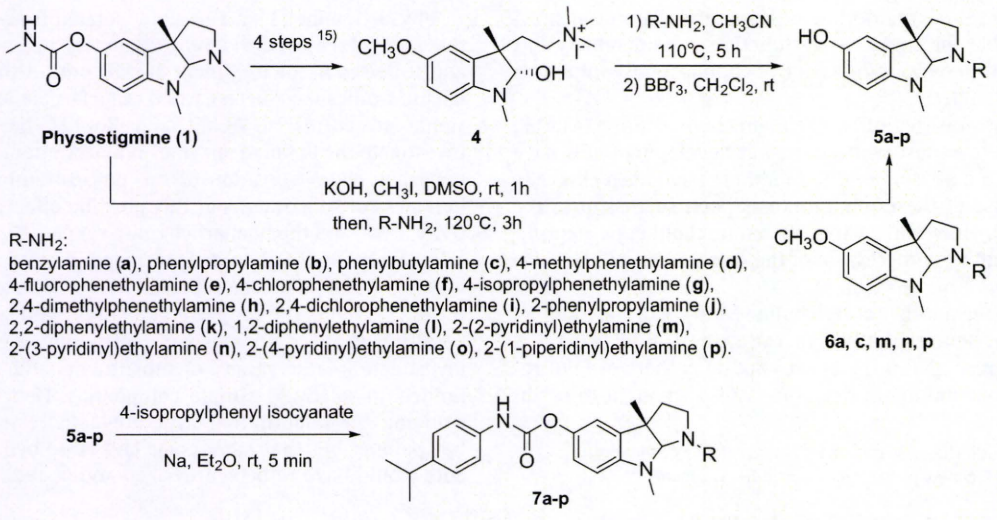

Scheme 1.

Table 1
Anti-ChE activity and enzyme selectivity

Compounds	R	AChE[a] (nM)	BuChE[a] (nM)	Selectivity[b]
1	Methyl (methylcarbamate, physostigmine)	40	280	0.14
7a	Benzyl	>100,000	510	>196
2	Phenethyl	>100,000	540	>185
7b	Phenylpropyl	>100,000	510	>196
7c	Phenylbutyl	>100,000	550	>182
7d	4-Methylphenethyl	>100,000	730	>137
7e	4-Fluorophenethyl	>100,000	500	>200
7f	4-Chlorophenethyl	>100,000	500	>200
3	Methyl	8400	240	35
7g	4-Isopropylphenethyl	>100,000	3300	>30
7h	2,4-Dimethylphenethyl	>100,000	1100	>91
7i	2,4-Dichlorophenethyl	>100,000	2600	>38
7j	2-Phenylpropyl	>100,000	720	>139
7k	2,2-Diphenylethyl	>100,000	10,000	>10
7l	1,2-Diphenylethyl	>100,000	15,000	>7
7m	2-(2-Pyridinyl)ethyl	4200	160	26
7n	2-(3-Pyridinyl)ethyl	>100,000	180	>556
7o	2-(4-Pyridinyl)ethyl	23,000	170	135
7p	2-(1-Piperidinyl)ethyl	3500	170	21

[a] In order to estimate the enzyme activity, changes in the absorbance at 2 min intervals were measured at 415 nm using a spectrophotometer. The enzyme activity is expressed as a percent of the activity of the solvent, DMSO. Seven different concentrations of each compound were used and the IC_{50} values of each compound were calculated by nonlinear regression of the sigmoidal dose-response curve using GraphPad Prism version 4.03. Only the results with correlation coefficients of $r^2 \geqslant 0.95$ were accepted. The results are represented as the mean of the IC_{50} obtained from at least four independent measurements.

[b] The selectivity was calculated as follows; selectivity = IC_{50} AChE/IC_{50} BuChE.

of fit, Q^2 is the cross-validated R^2, S is the standard error, and F is the ratio of the variance of the calculated values to that of the observed values. Among the descriptors, log$S$ was the relatively most important factor and was positively correlated to the anti-BuChE activity. This descriptor might be greatly influenced by the result that the four most active compounds had an ionizable nitrogen in their N^1-substituents. Interestingly, a report previously described that less hydrophobic substituents are favorable,[13] consistent with our result, although the former report focused on the anti-AChE activity. Since it is considered that a part of the tricyclic moiety itself interacts with Trp82 in the choline binding site (or anionic site), it is not known how the ionizable nitrogen of pyridine or piperidine interacts with BuChE, but it appears to be beneficial to have the polar atom in the N^1 substituent. Moreover, weinerPol descriptor was negatively correlated with the anti-BuChE activity. Since this value is defined as the number of carbon atoms pairs that are separated by three carbon–carbon bonds, its value is generally larger in the branched alkane than in the linear alkane. Namely, this descriptor indicates that branched or spatially bulky substituents might be unfavorable.

In summary, by synthesizing various norcymserine derivatives substituted on the N^1 moiety, and by performing the QSAR study, we found that pyridinylethyl and piperidinylethyl group substitution increased the anti-BuChE activity, and that the ionizable nitrogen of the substituent might contribute to this improvement.

Acknowledgment

This work was financially supported by Eisai Co., Ltd.

References and notes

1. Ferri, C.; Prince, M.; Brayne, C.; Brodaty, H.; Fratiglioni, L.; Ganguli, M.; Hall, K.; Hasegawa, K.; Hendrie, H.; Huang, Y.; Jorm, A.; Mathers, C.; Menezes, P.; Rimmer, E.; Scazufca, M. *Lancet* **2005**, *366*, 2112.
2. Giacobini, E. *Int. J. Geriatr. Psychiatry* **2003**, *18*, S1.
3. Wright, C.; Geula, C.; Mesulam, M. *Ann. Neurol.* **1993**, *34*, 373.
4. Greig, N.; Utsuki, T.; Ingram, D.; Wang, Y.; Pepeu, G.; Scali, C.; Yu, Q.; Mamczarz, J.; Holloway, H.; Giordano, T.; Chen, D.; Furukawa, K.; Sambamurti, K.; Brossi, A.; Lahiri, D. *Proc. Natl. Acad. Sci. U.S.A.* **2005**, *102*, 17213.
5. Li, B.; Duysen, E.; Carlson, M.; Lockridge, O. *J. Pharmacol. Exp. Ther.* **2008**, *324*, 1146.
6. Primo-Parmo, S.; Bartels, C.; Wiersema, B.; van der Spek, A.; Innis, J.; La Du, B. *Am. J. Hum. Genet.* **1996**, *58*, 52.
7. Sussman, J.; Harel, M.; Frolow, F.; Oefner, C.; Goldman, A.; Toker, L.; Silman, I. *Science* **1991**, *253*, 872.
8. Nicolet, Y.; Lockridge, O.; Masson, P.; Fontecilla-Camps, J.; Nachon, F. *J. Biol. Chem.* **2003**, *278*, 41141.
9. Pei, X.; Greig, N.; Bi, S.; Brossi, A. *Med. Chem. Res.* **1995**, *5*, 455.
10. Yu, Q.; Pei, X.; Holloway, H.; Greig, N.; Brossi, A. *J. Med. Chem.* **1997**, *40*, 2895.
11. Yu, Q.; Greig, N.; Holloway, H.; Brossi, A. *J. Med. Chem.* **1998**, *41*, 2371.
12. Yu, Q.; Holloway, H.; Utsuki, T.; Brossi, A.; Greig, N. *J. Med. Chem.* **1999**, *42*, 1855.
13. Kaur, J.; Zhang, M. *Curr. Med. Chem.* **2000**, *7*, 273.
14. Brzostowska, M.; He, X.; Greig, N.; Rapoport, S.; Brossi, A. *Med. Chem. Res.* **1992**, *2*, 238.
15. Pei, X.; Greig, N.; Flippen-Anderson, J.; Bi, S.; Brossi, A. *Helv. Chim. Acta* **1994**, *77*, 1412.
16. Yu, Q.; Brossi, A. *Heterocycles* **1988**, *27*, 745.
17. Yu, Q.; Luo, W.; Holloway, H.; Utsuki, T.; Perry, T.; Lahiri, D.; Greig, N.; Brossi, A. *Heterocycles* **2003**, *61*, 529.
18. Ellman, G.; Courtnry, K.; Andres, V. J.; Feather-Stone, R. *Biochem. Pharmacol.* **1961**, *7*, 88.
19. Recanatini, M.; Cavalli, A.; Hansch, C. *Chem. Biol. Interact.* **1997**, *105*, 199.
20. Wiener, H. *J. Am. Chem. Soc.* **1947**, *69*, 17.
21. Oprea, T. *J. Comput. Aided Mol. Des.* **2000**, *14*, 251.

nature medicine

Salt-sensitive hypertension in circadian clock–deficient *Cry*-null mice involves dysregulated adrenal Hsd3b6

Masao Doi[1], Yukari Takahashi[1], Rie Komatsu[1], Fumiyoshi Yamazaki[1], Hiroyuki Yamada[1], Shogo Haraguchi[2], Noriaki Emoto[3], Yasushi Okuno[4], Gozoh Tsujimoto[5], Akihiro Kanematsu[6], Osamu Ogawa[6], Takeshi Todo[7], Kazuyoshi Tsutsui[2], Gijsbertus T J van der Horst[8] & Hitoshi Okamura[1]

Malfunction of the circadian clock has been linked to the pathogenesis of a variety of diseases. We show that mice lacking the core clock components Cryptochrome-1 (Cry1) and Cryptochrome-2 (Cry2) (*Cry*-null mice) show salt-sensitive hypertension due to abnormally high synthesis of the mineralocorticoid aldosterone by the adrenal gland. An extensive search for the underlying cause led us to identify type VI 3β-hydroxyl-steroid dehydrogenase (Hsd3b6) as a new hypertension risk factor in mice. *Hsd3b6* is expressed exclusively in aldosterone-producing cells and is under transcriptional control of the circadian clock. In *Cry*-null mice, *Hsd3b6* messenger RNA and protein levels are constitutively high, leading to a marked increase in 3β-hydroxysteroid dehydrogenase-isomerase (3β-HSD) enzymatic activity and, as a consequence, enhanced aldosterone production. These data place Hsd3b6 in a pivotal position through which circadian clock malfunction is coupled to the development of hypertension. Translation of these findings to humans will require clinical examination of human *HSD3B1* gene, which we found to be functionally similar to mouse *Hsd3b6*.

Hypertension is a complex trait, influenced by multiple genetic and environmental factors[1]. Although it has been estimated that approximately 30–50% of blood pressure variance is due to inherited genes, the molecular basis of this disease remains largely to be defined[2]. In mammals, behavior, physiology and metabolism are subject to a well-controlled daily rhythm, generated by an internal self-sustained molecular oscillator referred to as the circadian clock[3–7]. Because up to 10% of the transcriptome has been estimated to be under the control of the circadian clock[8], it may not come as a surprise that malfunction of this time keeper can result in the onset of a variety of pathological events[9,10]. Indeed, epidemiological studies show that shift workers, long-distance transmeridian flight crews and individuals with sleep disorders show a higher than average prevalence of cardiovascular diseases[11–13]. Thus, it has been speculated that impediment of the circadian clock may underlie altered cardiovascular homeostasis. However, the molecular mechanisms by which circadian clock malfunction contribute to cardiovascular disease, including hypertension, are poorly understood.

Cry-null mice lack a functional circadian clock and accordingly show arrhythmic behavior, physiology and metabolism[14–16]. Cry proteins act as potent transcriptional repressors that downregulate transcription of E-box (CACGTG) enhancer–containing clock genes (including the Period- and Cryptochrome-encoding genes), as well as a wide variety of clock-controlled genes (including the gene encoding the circadian transactivator Dbp)[16–18]. Time of day–dependent activation and repression of such E-box–containing genes are central features of normal circadian clock function. In *Cry*-null mice, the expression of E-box–containing genes is constitutively increased (derepressed) as a result of impaired circadian repression[16,19,20].

To date, little is known about the pathological states of *Cry*-null mice. We and others have focused on the adrenal gland in investigating how the circadian clock system affects metabolism[21,22]. In characterizing the endocrinological status of *Cry*-deficiency mice, we found abnormally high levels of aldosterone, a steroid hormone that is secreted by the adrenal glands. Aldosterone acts as a potent mineralocorticoid that promotes sodium and water retention by the kidney, thereby increasing vascular fluid volume and blood pressure[23,24]. The plasma aldosterone concentration (PAC) is finely controlled by the renin-angiotensin-aldosterone system (RAAS), which regulates cardiovascular function and blood pressure homeostasis[2]. Because abnormal elevation of PAC has been linked to the pathogenesis of human hypertension[23–25], our observation of increased PAC in *Cry*-null mice prompted us to investigate how the circadian clock might be linked to the etiology of aldosterone-dependent disorders.

Here we show that *Cry*-null mice have salt-sensitive hypertension due to the abnormal production of aldosterone by the adrenal glands. An extensive search for a steroidogenic enzyme that causes the adrenal dysfunction in *Cry*-null mice led us to identify Hsd3b6 as a key

[1]Department of Systems Biology, Graduate School of Pharmaceutical Sciences, Kyoto University, Sakyo-ku, Kyoto, Japan. [2]Laboratory of Integrative Brain Sciences, Department of Biology, Faculty of Education and Integrated Arts and Sciences, Waseda University, Shinjuku-ku, Tokyo, Japan. [3]Division of Cardiovascular and Respiratory Medicine, Department of Internal Medicine, Kobe University Graduate School of Medicine, Chuo-ku, Kobe, Japan. [4]Department of Systems Bioscience for Drug Discovery, [5]Department of Genomic Drug Discovery Science, Graduate School of Pharmaceutical Sciences and [6]Department of Urology, Graduate School of Medicine, Kyoto University, Sakyo-ku, Kyoto, Japan. [7]Department of Radiation Biology and Medical Genetics, Graduate School of Medicine, Osaka University, Yamadaoka, Suita, Japan. [8]Department of Genetics, Center for Biomedical Genetics, Erasmus University Medical Center, Rotterdam, The Netherlands. Correspondence should be addressed to H.O. (okamurah@pharm.kyoto-u.ac.jp).

Received 9 July; accepted 26 October; published online 13 December 2009; doi:10.1038/nm.2061

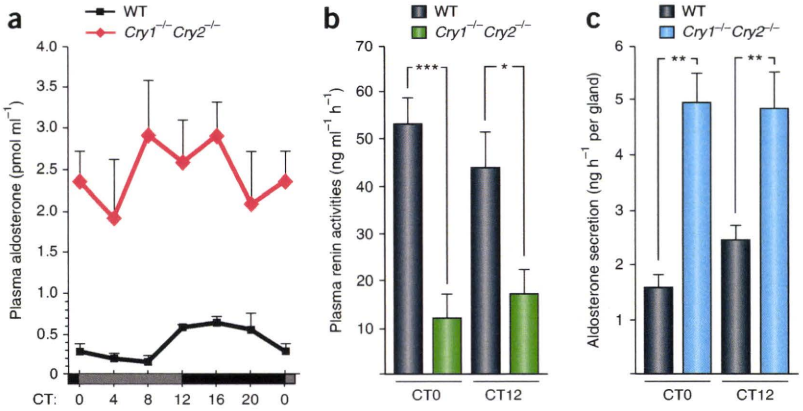

Figure 1 Overproduction of aldosterone by *Cry*-null adrenal glands. (**a**) Twenty-four–hour profiles of PAC in WT and *Cry*-null mice in constant darkness (n = 5–12 mice per time point). The values at CT0 are double plotted. (**b**) Plasma renin activity in WT and *Cry*-null mice at CT0 and CT12 (n = 6 mice per time point). (**c**) Aldosterone secretion from *ex vivo* tissue slices of adrenal glands collected from WT and *Cry*-null mice at CT0 and CT12 (CT0: WT, n = 6, *Cry*-null, n = 6; CT12: WT, n = 12, *Cry*-null, n = 10). Shown are the amounts of aldosterone secreted into serum-free medium during a 60-min incubation at 37 °C. Values in **a**–**c** are means ± s.e.m. $*P < 0.05$; $**P < 0.01$; $***P < 0.001$.

enzyme through which *Cry* gene inactivation results in an abnormally high PAC and salt-sensitive hypertension. Furthermore, we show that the human *HSD3B1* gene is a functional counterpart to the mouse *Hsd3b6* gene, as *HSD3B1* is expressed in aldosterone-producing cells in the human adrenal gland.

RESULTS

Chronic hyperproduction of aldosterone by *Cry*-null adrenal glands

After our initial observation of increased PAC in *Cry*-null mice, we quantified PAC and plasma renin activity (PRA) in wild-type (WT) and mutant mice kept in constant darkness and sampled at selected circadian time points (**Fig. 1**). *Cry*-null mice showed abnormally high PAC throughout the day (**Fig. 1a**). In line with previous reports in rodents[26], WT mice showed a mild circadian fluctuation in PAC (**Fig. 1a**) with overall values lower than those in *Cry*-null mice. The elevated PAC in *Cry*-null mice was not a secondary result of enhanced PRA, as PRA was markedly suppressed in *Cry*-null mice at both CT0 and CT12 (defined as the beginning of the subjective day and night, respectively) (**Fig. 1b**). The decreased PRA in *Cry*-null mice is most likely due to RAAS-dependent feedback inhibition resulting from the elevated PAC[23,24].

The increased PAC despite a marked reduction of PRA suggested that the functioning of the adrenal gland in *Cry*-null mice might be affected. To assess the functionality of the *Cry*-null adrenal gland, we used an *ex vivo* tissue culture system that allowed us to evaluate the rate of aldosterone production by measuring the amount of aldosterone secreted into the culture medium. We found that the aldosterone production rate of the *Cry*-null adrenal gland was significantly higher than that of the WT adrenal gland (**Fig. 1c**). This increased aldosterone production was observed in both adrenal glands of a *Cry*-null mouse (**Supplementary Fig. 1**). Taken together, these data provide evidence that *Cry*-null mice have a profoundly increased PAC as a result of enhanced aldosterone secretion by the adrenal gland.

Chronic hyperexpression of *Hsd3b6* in *Cry*-null adrenal glands

To dissect the altered steroidogenesis in *Cry*-null mice at the molecular level, we used microarrays to survey all known mouse steroidogenic genes for their expression in the adrenal gland (**Fig. 2a**). This survey identified a gene probe (1460232_s_at) for which signal intensities in the *Cry*-null adrenal gland were markedly increased throughout the day as compared to the WT gland. This gene probe potentially hybridizes with the *Hsd3b2*, *Hsd3b3* and *Hsd3b6* mRNA isoforms of the *Hsd3b* gene family. These isoforms are known to encode dehydrogenase-isomerases that catalyze the conversion of Δ^5-3β-hydroxysteroids into hormonally active Δ^4-3-ketosteroids[27], an enzymatic reaction required for aldosterone biosynthesis[28].

To identify all *Hsd3b* isoforms expressed in the mouse adrenal gland, we used an RT-PCR–based assay in combination with restriction endonuclease-mapping analysis (**Supplementary Methods**). We subjected adrenal total RNA to RT-PCR with a primer set capable of amplifying all classes of mouse *Hsd3b* genes (types I to VI). We then analyzed the identity of the PCR products by digestion of the DNA with subtype-specific restriction endonucleases (**Supplementary Table 1**). We observed that mouse adrenal glands express only type I and VI *Hsd3b* isoforms; the other isoforms (types II to V) were undetectable (**Supplementary Fig. 2**). Quantitative RT-PCR (qRT-PCR) analysis with gene-specific primers further showed that the *Hsd3b* gene aberrantly expressed in *Cry*-null adrenal glands was *Hsd3b6* rather than *Hsd3b1*; that *Hsd3b6* mRNA levels in *Cry*-null adrenal glands were constitutively increased compared to those in WT adrenal glands across circadian time; and that *Hsd3b6* expression in WT adrenal glands, although at relatively low levels, was subject to circadian fluctuation (**Fig. 2b**). *In vitro* promoter analysis (**Supplementary Fig. 3a**) revealed that the transcription of *Hsd3b6* is positively controlled by Dbp, suggesting that the enhanced Dbp expression in *Cry*-null mice (refs. 17 and 20 and **Supplementary Fig. 3b**) could account for the hyperexpression of *Hsd3b6* in *Cry*-null adrenal glands (**Supplementary Fig. 3c,d**).

Hsd3b6 is exclusively expressed in zona glomerulosa cells

In situ hybridization analysis with a radiolabeled *Hsd3b6* probe (**Fig. 2c**) not only confirmed the marked elevation of *Hsd3b6* mRNA in *Cry*-null adrenal glands but also uncovered a unique spatial arrangement of *Hsd3b6* expression. This analysis showed that *Hsd3b6* is expressed almost exclusively in the outer layer of the adrenal cortex (**Fig. 2c** and **Supplementary Fig. 4**). Analysis of *Hsd3b6* expression by emulsion autoradiography (data not shown) and digoxigenin *in situ* hybridization (**Supplementary Fig. 5a**) further illustrated that the *Hsd3b6*-positive cells were localized in the outermost cortical layer, termed the zona glomerulosa.

The predominant expression of *Hsd3b6* in the zona glomerulosa is particularly noteworthy because the production of aldosterone is known to take place exclusively in this region[29]. The zona glomerulosa is functionally characterized by the expression of the *Cyp11b2* gene, which encodes the aldosterone synthase required for the final step of aldosterone synthesis[30,31]. Notably, our *in situ* hybridization analysis suggested that *Hsd3b6* and *Cyp11b2* are both expressed mainly in adrenal zona glomerulosa cells (**Fig. 2c** and **Supplementary Fig. 5b**). In marked contrast to the local expression of *Hsd3b6*, *Hsd3b1* was expressed more broadly in the adrenal cortex (**Fig. 2c**), similar to

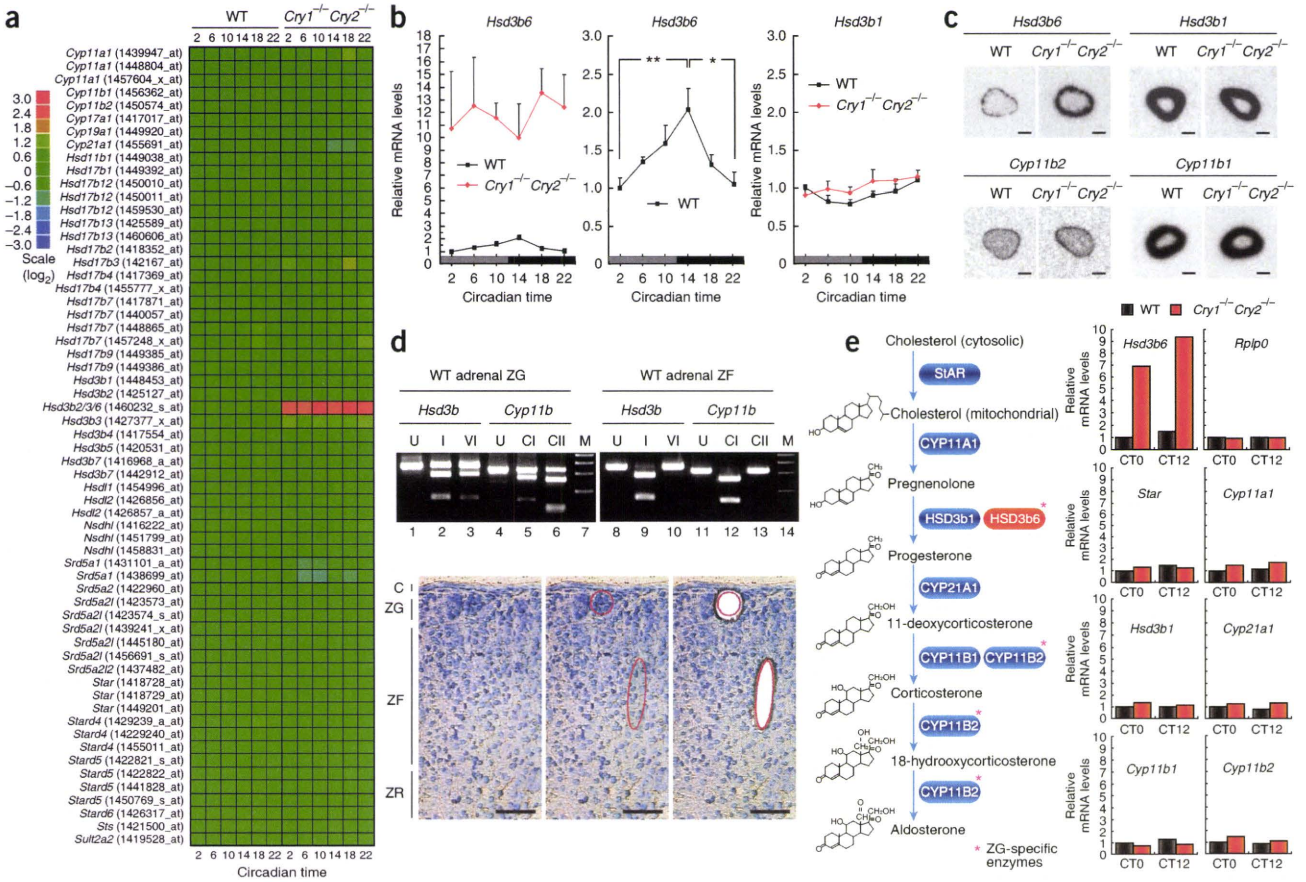

Figure 2 Chronically high expression of *Hsd3b6* in aldosterone-producing zona glomerulosa (ZG) cells of *Cry*-null adrenal glands. (**a**) Twenty-four–hour expression profiles of steroidogenic genes in WT and *Cry*-null adrenal glands. The relative levels of each transcript, determined by DNA microarray analysis, are indicated by the color scale. For each transcript, values were normalized to the average expression level over the day in WT adrenal glands. The identity of each transcript is indicated by the Affymetrix probe used and the gene symbol (see also gene names shown in the **Supplementary Methods**) except that three isoforms of the *Hsd3b* gene (*Hsd3b2*, *Hsd3b3* and *Hsd3b6*), to which the gene probe 1460232_s_at can hybridize, are denoted as *Hsd3b2/3/6*. (**b**) qRT-PCR–verified 24-h expression profiles of *Hsd3b6* and *Hsd3b1* in WT and *Cry*-null adrenal glands. Values are means ± s.e.m. ($n = 5$ mice for each data point) normalized to expression of TATA-box binding protein (Tbp)-encoding gene. The middle graph is an expanded version of the left graph to more clearly show the circadian rhythmicity (phase and amplitude) of *Hsd3b6* expression in WT adrenal glands. $^{*}P < 0.05$; $^{**}P < 0.01$. (**c**) Radioisotopic *in situ* hybridization autoradiographs for *Hsd3b6*, *Hsd3b1*, *Cyp11b2* and *Cyp11b1* in WT and *Cry*-null adrenal glands collected at CT0. Scale bars, 0.5 mm. (**d**) Zonal expression of *Hsd3b* and *Cyp11b* isoforms. cDNA fragments of *Hsd3b* and *Cyp11b* were amplified from either ZG or zona fasciculata (ZF) cells as indicated and were enzymatically digested with isoform-specific restriction endonucleases. I, digestion with AccI; VI, NdeI; CI, NheI; CII, SacI. U, undigested; M, DNA marker. The micrographs show a representative tissue section before and after laser microdissection. ZG cells are ovoid in shape and are arranged in globular clusters, lying directly beneath the capsular layer. C, capsule; ZR, zona reticularis. Toluidine blue staining. Scale bars, 50 μm. The data shown in **c** and **d** are representative of three or more independent experiments. (**e**) Left, schematic of the aldosterone biosynthetic pathway. Right, qRT-PCR analysis of the expression of genes involved in aldosterone biosynthesis in WT and *Cry*-null ZG cells at CT0 and CT12 ($n = 4$ adrenal glands for each cDNA preparation). Values are expressed as the mean of two independent experiments, which yielded equivalent results. *Rplp0* is a nonoscillating abundant gene, the expression of which reflects the total amount of RNA used.

expression of the *Cyp11b1* gene, which encodes the steroid 11β-hydroxylase involved in the production of corticosterone[30,32]. These data thus disclose a previously uncharacterized spatial and functional separation between *Hsd3b6* and *Hsd3b1* in the mouse adrenal gland.

To further confirm the local expression of *Hsd3b6* in zona glomerulosa cells, we generated an antibody to Hsd3b6 and performed immunohistochemistry (**Fig. 3**). Notably, almost all zona glomerulosa cells in the *Cry*-null adrenal gland were found to be immunoreactive to the Hsd3b6-specific antibody (**Fig. 3a**). To determine whether *Cyp11b2* is coexpressed with Hsd3b6, we further processed immunostained adrenal sections for *in situ* hybridization with a digoxigenin-labeled *Cyp11b2* probe. This double-labeling analysis revealed that nearly all Hsd3b6-positive cells also expressed *Cyp11b2* (**Fig. 3b**). The converse was also true; almost all *Cyp11b2*-positive cells were Hsd3b6-immunopositive (**Fig. 3b**). This high degree of colocalization of Hsd3b6 protein with the aldosterone synthase *Cyp11b2* mRNA strongly suggests that the zona glomerulosa–specific Hsd3b6 isoform is involved in aldosterone production in the mouse adrenal gland.

Steroidogenic genes in *Cry*-null zona glomerulosa cells

As the zona glomerulosa cell population constitutes only a fraction of the total number of adrenal gland cells, assays using whole adrenal gland (**Supplementary Fig. 2**) could lead to an underestimation of *Hsd3b6* expression in this tissue. Indeed, probably because of

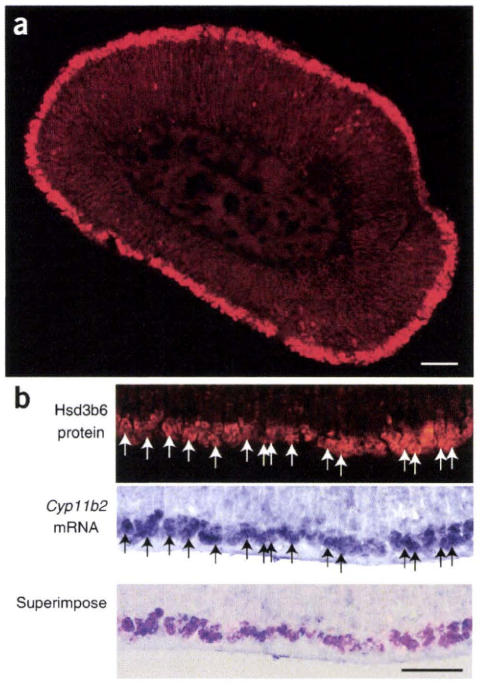

Figure 3 Coexpression of Hsd3b6 protein and *Cyp11b2* mRNA in adrenal zona glomerulosa cells. (**a**) Immunocytochemistry of Hsd3b6 protein in a *Cry*-null adrenal gland. Scale bar, 100 μm. (**b**) Double labeling of Hsd3b6 protein and *Cyp11b2* transcript. Immunostained adrenal sections were subsequently subjected to *in situ* hybridization with a digoxigenin-labeled *Cyp11b2* probe. Shown are higher magnification views of a region containing zona glomerulosa cells. Nearly all zona glomerulosa cells express both Hsd3b6 (red) and *Cyp11b2* (blue). Arrows indicate representative double-labeled cells. Scale bar, 100 μm. The data are representative of three or more independent experiments.

this reason, the presence of adrenal *Hsd3b6* has been left undefined to date[27,28]. We next carried out laser microdissection to examine in more detail the zonal expression of *Hsd3b6* and *Hsd3b1* in the WT adrenal gland. (**Fig. 2d**). Cells in either the zona glomerulosa or the zona fasciculata (a middle layer of the adrenal cortex) were separately excised by laser microdissection; total RNA extracts from these cells were then analyzed by RT-PCR with a primer set that can amplify both *Hsd3b1* and *Hsd3b6* (the sequence similarity between these two genes enabled amplification of both genes with a common primer set). Subtype-specific DNA digestion revealed almost equivalent concentrations of *Hsd3b1* and *Hsd3b6* mRNA in the zona glomerulosa cells (**Fig. 2d**), suggestive of a substantial role of Hsd3b6 in aldosterone production by WT adrenal glands. Of note, *Hsd3b6* was zona glomerulosa specific, with virtually no expression in zona fasciculata cells, whereas *Hsd3b1* was predominantly expressed in zona fasciculata cells (**Fig. 2d**). A similar examination of subtype-specific expression of *Cyp11b* genes showed that, like *Hsd3b6*, expression of *Cyp11b2* was confined to zona glomerulosa cells (**Fig. 2d** and **Supplementary Table 2**). These observations confirm the cellular purity of our laser microdissection samples and provide further evidence of the colocalization of *Hsd3b6* and *Cyp11b2* expression in zona glomerulosa cells.

We also performed qRT-PCR analysis on zona glomerulosa cell–specific RNA preparations and confirmed that the *Hsd3b6* mRNA level was drastically increased in *Cry*-null zona glomerulosa cells as compared to WT cells (**Fig. 2e**). We did not observe such elevated expression for transcripts of other steroidogenic genes tested (*Star* (encoding steroidogenic acute regulatory protein), *Cyp11a1*, *Hsd3b1*, *Cyp21a1*, *Cyp11b1* and *Cyp11b2*) (**Fig. 2e**).

Chronically enhanced 3β-HSD activity in *Cry*-null mice

If the observed increase in the levels of *Hsd3b6* mRNA is functionally relevant, it should be accompanied by increased accumulation of Hsd3b6 protein in *Cry*-null adrenal glands. Immunoblot analysis revealed that the amount of Hsd3b6 protein in the *Cry*-null adrenal gland was highly elevated at both CT0 and CT12, whereas the amount of Cyp11a1 protein remained unchanged (**Fig. 4a**). Next, we assayed 3β-HSD enzymatic activity in WT and *Cry*-null enucleated adrenal glands (that is, the capsular portion of the glands), which consist mainly of zona glomerulosa cells. At both CT0 and CT12, we observed a marked increase of 3β-HSD activity in enucleated adrenal glands from *Cry*-null mice compared to WT mice, regardless of the 3β-HSD substrate used (**Fig. 4b**). In contrast, 3β-HSD activity in the decapsulated portion of the adrenal gland (containing the zona fasciculata, zona reticularis and medulla) was essentially unaffected in *Cry*-null mice (**Supplementary Fig. 6**). These results indicate that an elevation of 3β-HSD activity accompanies the accumulation of Hsd3b6 protein observed in aldosterone-producing zona glomerulosa cells.

We next examined whether pharmacological inhibition of 3β-HSD enzymatic activity *in vivo* by treatment of mice with trilostane[33] leads to a reduction in the PAC in *Cry*-null mice. The PAC in WT mice remained nearly unchanged by trilostane treatment even at a relatively high standard dose (8 mg per kg body weight per d) (**Fig. 4c**). The apparent tolerance of WT mice to trilostane treatment has

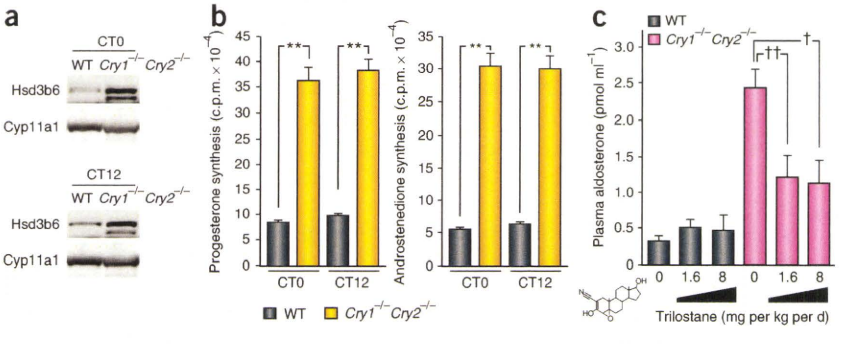

Figure 4 Elevated 3β-HSD activity is responsible for aldosterone overproduction in *Cry*-null mice. (**a**) Immunoblot analysis of Hsd3b6 and Cyp11a1 proteins in microsomal protein extracts from WT and *Cry*-null adrenal glands isolated at CT0 and CT12 ($n = 4$ adrenal glands for each time point). Similar data were acquired in two independent experiments. (**b**) 3β-HSD enzymatic activity in the zona glomerulosa cell layer–containing capsular portion of WT and *Cry*-null adrenal glands at CT0 and CT12. Left, progesterone synthesis from ^{3}H-pregnenolone; right, androstenedione synthesis from ^{3}H-dehydroepiandrosterone. We used one adrenal gland per assay. Values are means ± s.e.m. ($n = 12$ assays for each data point). $^{**}P < 0.0001$. (**c**) PACs in WT and *Cry*-null mice at CT0 after daily administration of the 3β-HSD inhibitor trilostane at the indicated doses for 7 d ($n = 6$ mice for each dose). Values are means ± s.e.m. $^{\dagger}P = 0.01$; $^{\dagger\dagger}P = 0.02$.

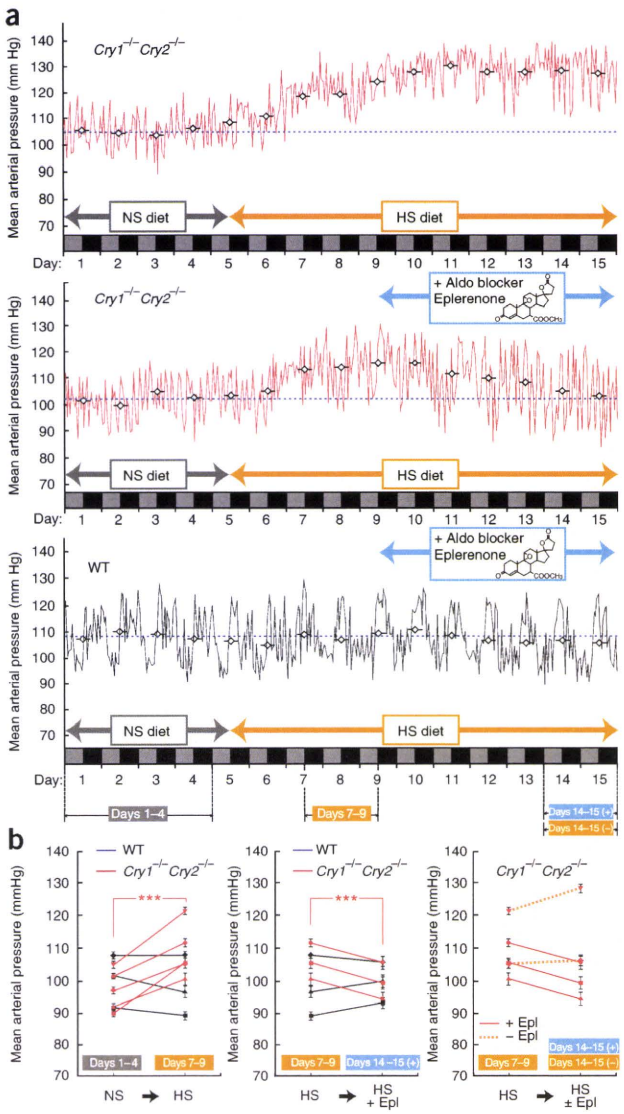

Figure 5 *Cry*-null mice show salt-sensitive hypertension. (**a**) Representative recordings of 15-d temporal profiles of mean arterial blood pressure of WT and *Cry*-null mice. Mice were kept in constant darkness and fed either normal salt diet (NS; 0.2% sodium) or high-salt diet (HS; 3.15% sodium) on the days indicated by gray and yellow arrows, respectively. Blue arrows indicate the period during which the HS diet contained eplenerone (Epl). Gray and black boxes below the graphs represent the subjective day and subjective night, respectively. Blood pressure data were collected in 30-s bouts at 5-min intervals and plotted using a 1-h moving average. The 24-h means of each day are shown by open squares. Horizontal dotted lines indicate the mean value of the blood pressure at days 1–4 on NS diet. (**b**) Pair-wise comparisons of blood pressures before and after HS diet (left), before and after Epl treatment (middle) and with or without Epl on HS diet (right). Plotted are the blood pressures of individual mice (WT, $n = 3$; *Cry*-null, $n = 5$; two of the *Cry*-null mice were used as non-Epl controls). Values are means ± s.e.m. $^{***}P < 0.001$, paired comparison in *Cry*-null mice.

been considered to result from feedback regulation by the RAAS[34]. In marked contrast, trilostane treatment was effective in suppressing the increased PAC in *Cry*-null mice (**Fig. 4c**), in which the constitutive overproduction of aldosterone reflects its independence from normal RAAS control. These data are consistent with the idea that the highly elevated 3β-HSD activity in zona glomerulosa cells of *Cry*-null mice contributes to the elevated PAC of these mice.

Aldosterone-dependent hypertension in *Cry*-null mice

We next explored the pathological consequences of excessive aldosterone in *Cry*-null mice. As a finely controlled RAAS is crucial to blood pressure homeostasis, we compared blood pressure in WT and *Cry*-null mice (**Fig. 5**). We monitored daily changes in the mean arterial blood pressure in constant darkness by radiotelemetry (**Supplementary Methods**). The circadian variation in blood pressure characteristic for WT mice was completely lost in *Cry*-null mice (**Fig. 5a**). However, when averaged over 24 h, blood pressure in WT and *Cry*-null mice appeared similar under standard conditions (**Fig. 5b**).

Because mineralocorticoid aldosterone-dependent hypertension may be influenced by dietary salt intake[23,24], we next examined the salt sensitivity of blood pressure in WT and mutant mice. Normally, blood pressure is resilient to variations in sodium ingestion due to homeostatic control by RAAS. Indeed, blood pressure in WT mice ($n = 3$) was unaffected by the switch from a normal-salt to a high-salt diet (**Fig. 5a,b**; normal-salt, 100.3 ± 7.8 (s.d.) mmHg; high salt, 97.9 ± 9.4 mm Hg), associated with a marked reduction of PAC upon the high-salt loading (**Supplementary Fig. 7**). In contrast, *Cry*-null mice became hypertensive in a salt-dependent manner (**Fig. 5a**). All mutant mice tested ($n = 5$) experienced a drastic increase in blood pressure within 2 d after the change to the high-salt diet (**Fig. 5b**; normal-salt, 97.2 ± 6.3 (s.d.) mmHg; high-salt, 108.8 ± 7.9 mm Hg; $P < 0.001$, paired t test). The PAC of these mice remained relatively high even after the high-salt loading (**Supplementary Fig. 7**). The excess of circulating aldosterone indeed contributed to the elevation of blood pressure, as the high-salt–induced hypertension in *Cry*-null mice ($n = 3$) could be reversed by treatment with eplerenone, a selective aldosterone blocker[35] (**Fig. 5a,b**; before eplerenone, 106.7 ± 5.5 (s.d.) mmHg; after eplerenone, 99.6 ± 5.3 mm Hg; $P < 0.001$, paired t test). The observed decrease in blood pressure was not due to salt desensitization induced by long-term high-salt ingestion, as the blood pressure in *Cry*-null mice remained elevated while they were fed the high-salt diet (**Fig. 5a,b**). These data provide evidence for an aldosterone-dependent alteration of blood pressure homeostasis in *Cry*-null mice.

Human *HSD3B1* is a functional counterpart of mouse *Hsd3b6*

To begin to address the question of whether these findings have relevance for human idiopathic hypertensive disease[23,24], we tested whether the human adrenal gland also expresses a zona glomerulosa–specific *HSD3B* isoform. Nontumorous adrenal tissue from adrenalectomy specimens were obtained from two human subjects (2237N and 1774N) after written informed consent. cDNA cloning from zona glomerulosa cells and subsequent DNA sequencing analysis showed that the human *HSD3B1* gene, which has been considered a candidate human counterpart of the mouse *Hsd3b6* gene[27,28,36] (**Supplementary Table 3**) was expressed in the human adrenal zona glomerulosa samples tested (**Fig. 6a–d**).

Strikingly, human *HSD3B1* and *HSD3B2* show a high sequence similarity (93.6% identity, including the 5′ and 3′ untranslated regions; **Fig. 6a**). We thus developed subtype-specific Taqman minor groove binder (MGB) probes to allow us to distinguish these genes on the basis of nucleotide differences in the region encoding the dehydrogenase catalytic YXXXK motif[27] (where X is any amino acid): the third residue of the motif encodes histidine in *HSD3B1* and tyrosine in *HSD3B2* (**Fig. 6a**).

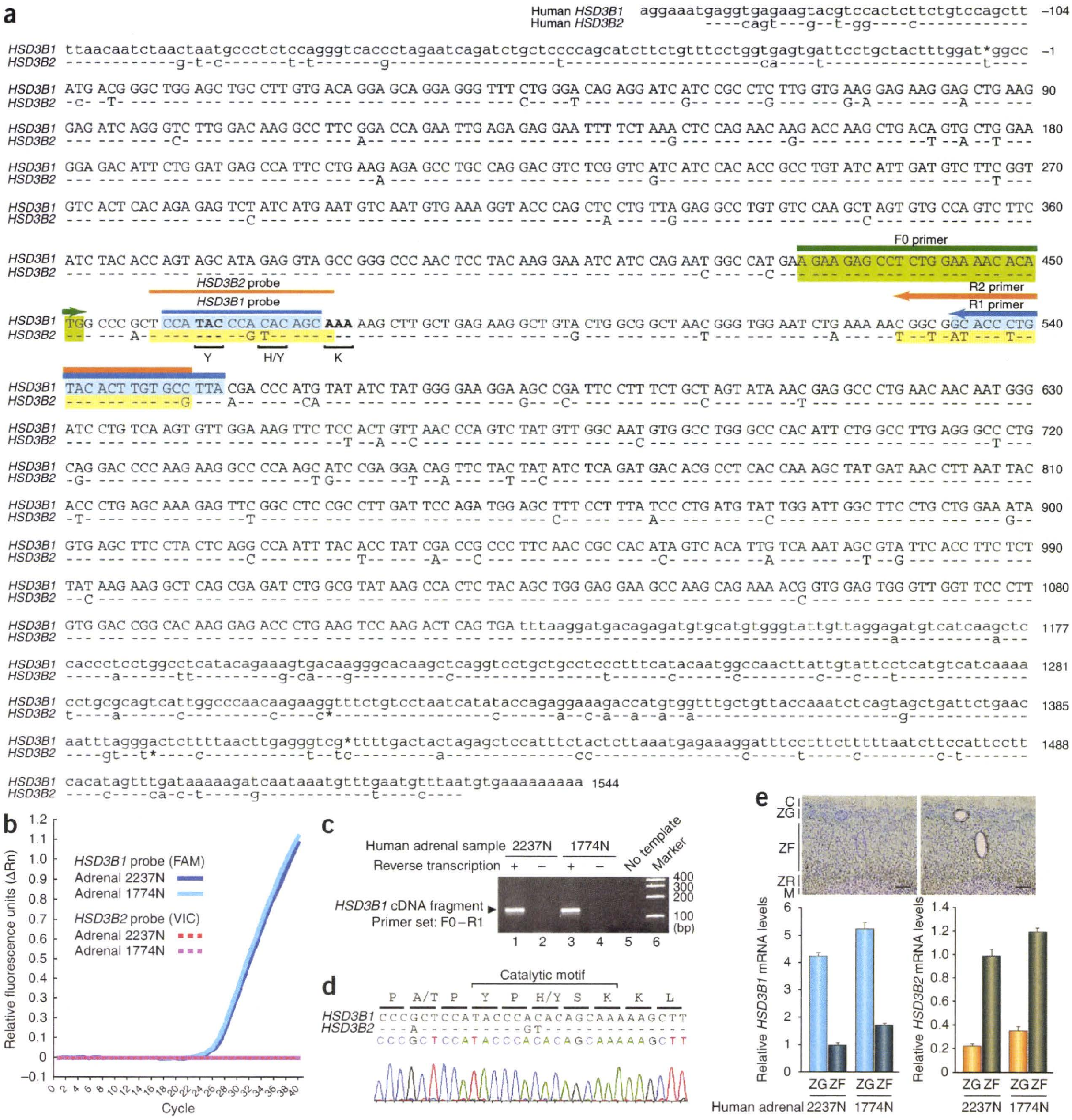

Figure 6 Identification of a zona glomerulosa–specific *HSD3B* isoform in the human adrenal gland. (**a**) cDNA sequences of human *HSD3B1* and *HSD3B2*. Uppercase letters represent nucleotides in the protein coding sequence, and lowercase letters represent the 5′ or 3′ untranslated regions. Hyphens indicate *HSD3B2* nucleotides that are common to *HSD3B1*. Asterisks indicate missing nucleotides. Shown in bold are the codons for tyrosine and lysine in the dehydrogenase catalytic YXXXK motif (X is any amino acid) with the third residue being subtype specific (histidine for *HSD3B1* and tyrosine for *HSD3B2*). Nucleotide numbering for *HSD3B1* is indicated. Blue and orange lines above the sequences indicate the probe regions for *HSD3B1* and *HSD3B2*, respectively. The F0 forward primer (green arrow) recognizes both isoforms, whereas R1 (blue arrow) and R2 (orange arrow) reverse primers are specific to *HSD3B1* and *HSD3B2*, respectively. (**b**) Real-time PCR fluorescence curves for quantification of *HSD3B1* mRNA. Zona glomerulosa cells collected from human adrenal samples 2237N and 1774N were subjected to qRT-PCR with F0 and R1 primers. cDNA amplification was readily observed for *HSD3B1* (FAM-labeled probe) but not for *HSD3B2* (VIC-labeled), showing the specificity of the Taqman probes. ΔRn, normalized reporter signal. Similar results were obtained in three independent measurements. (**c**,**d**) Analysis of cDNA fragments amplified with the F0 and R1 primers. (**c**) qRT-PCR products were separated by agarose gel electrophoresis. As a control, reverse transcriptase treatment was omitted in lanes 2 and 4. The arrowhead indicates the expected position (127 base pairs (bp)) of amplicons originating from *HSD3B1* transcripts. (**d**) A representative DNA sequence chromatograph of amplified cDNA fragments from sample 2237N, showing sequence corresponding to the catalytic motif that is unique to *HSD3B1*. (**e**) qRT-PCR analysis of *HSD3B1* and *HSD3B2*. The micrograph shows a representative laser microdissection section of the adrenal gland from subject 2237N. Scale bars, 100 μm. C, capsule; ZR, zona reticularis; M, medulla. Shown are mean concentrations ± s.d. (three independent measurements) of *HSD3B1* (left) and *HSD3B2* (right) in subjects 2237N and1774N. Values were normalized to the expression of *RPLPO* and plotted relative to expression in the zona fasciculata cells of subject 2237N.

Subtype-specific Taqman qRT-PCR analysis revealed that expression of human *HSD3B1* was considerably enriched in zona glomerulosa cells, as compared to zona fasciculata cells. Conversely, expression of human *HSD3B2* was predominantly expressed in zona fasciculata cells, suggesting that this gene is a counterpart of the mouse *Hsd3b1* gene (**Fig. 6e**). These observations support the notion that human *HSD3B1*, but not *HSD3B2*, represents a functional counterpart of the mouse *Hsd3b6* gene (**Supplementary Table 3**).

DISCUSSION

This study unveils a new aspect of circadian clock–related pathology: salt-sensitive hypertension. *Cry*-null mice show an adrenal disorder characterized by chronic overproduction of aldosterone that persists even in the reduced plasma renin activity. Our search for the pathogenic factor underlying this adrenal disorder led to the identification of Hsd3b6, which to our knowledge has not been previously associated with hypertension in rodents. The circadian clock governs the levels of daily expression of *Hsd3b6*. The impediment of the circadian clock could therefore be coupled to the development of hypertension through the abnormal regulation of Hsd3b6-dependent aldosterone synthesis in the adrenal gland.

How do our findings relate to human aldosterone-dependent hypertensive disease? Chronic overproduction of aldosterone by human adrenal zona glomerulosa cells, a disorder referred to as primary hyperaldosteronism, is clinically known to constitute a frequent form of secondary hypertension[23]. Primary hyperaldosteronism can be classified into two distinct diagnostic categories: aldosterone-producing adenoma and bilateral idiopathic hyperaldosteronism. Unlike aldosterone-producing adenoma, which has a known etiology that can be corrected by surgery, the pathophysiology underlying nontumorigenic idiopathic hyperaldosteronism remains totally unknown[24], as reflected in its being labeled 'idiopathic'. Idiopathic hyperaldosteronism does not allow for surgical correction by adrenalectomy because of its bilateral nature, and specific therapies to reduce aldosterone production are not available[23]. Despite the medical importance of this disorder, the underlying mechanisms have remained unexplored largely because of the lack of a suitable animal model.

Cry-null mice, in which circulating aldosterone is chronically overproduced by the adrenal glands, represent a promising animal model of idiopathic hyperaldosteronism. Our analysis of steroidogenic gene expression in *Cry*-null zona glomerulosa cells led to an unexpected finding. Whereas the rate-limiting step for aldosterone production by zona glomerulosa cells remains to be experimentally defined, previous studies suggested a key role for Cyp11b2, as the enhancement of aldosterone biosynthesis by angiotensin II is associated with an acute induction of *Cyp11b2* expression in zona glomerulosa cells[37]. However, we observed that *Cyp11b2* expression was essentially unimpaired in *Cry*-null mice, suggesting another molecular mechanism for aldosterone overproduction in *Cry*-null mice. We thus carried out a nonbiased examination of adrenal steroidogenic genes, which led to the identification of *Hsd3b6* as a new gene exclusively expressed in zona glomerulosa cells. Notably, the only effect on gene expression that we were able to detect in *Cry*-null adrenal glands was increased expression of zona glomerulosa–specific *Hsd3b6*; the expression of other steroidogenic genes tested was unaffected. Furthermore, elevation of Hsd3b6 protein abundance resulted in chronically enhanced 3β-HSD activity in *Cry*-null adrenal zona glomerulosa cells, and *in vivo* inhibition of 3β-HSD activity by trilostane was effective in suppressing the increased PAC in *Cry*-null mice. These data thus characterize mouse Hsd3b6 as a latent risk factor for hyperaldosteronism: chronic elevation of its activity in zona glomerulosa cells instigates an abnormal elevation of PAC.

It may be somewhat unexpected that zona glomerulosa–specific *HSD3B* gene expression by human *HSD3B1* and mouse *Hsd3b6* has escaped notice thus far. However, it should be noted that to show that human *HSD3B1* gene expression is specific to zona glomerulosa cells, we had to develop a Taqman MGB probe–based qPCR method that can distinguish between transcripts of the *HSD3B1* and *HSD3B2* genes. Notably, these two isoforms are indistinguishable by conventional probe hybridization methods because of their extremely high DNA sequence similarity. Furthermore, as the zona glomerulosa cell population constitutes only a fraction of the total number of adrenal gland cells, the levels of gene expression in this cell type might have been underestimated in assays using whole adrenal extracts[38,39]. Indeed, we observed that the expression of mouse *Hsd3b6* was apparently low when analyzed in whole adrenal RNA. By applying laser-microdissection technology, in combination with subtype-specific qRT-PCR, we were able to identify the zona glomerulosa–specific *HSD3B* genes in both human and mouse adrenal glands.

On the basis of these results, the potential involvement of the human *HSD3B1* gene in adrenal zona glomerulosa pathophysiology merits further investigation. Whereas numerous studies link mutations in human *HSD3B2* to 3β-HSD deficiency leading to impaired steroidogenesis in both the adrenal glands and the gonads[40,41], no human *HSD3B1* gene mutations have been observed in clinical screening of human postnatal disorders[27]. Human *HSD3B1* is expressed not only in the adrenal zona glomerulosa but also in the placenta, where HSD3B1 functions as the major 3β-HSD isoform for production of progesterone, which is vital for the maintenance of human pregnancy. It has therefore been suggested that, in a fetus homozygous for a *HSD3B1* gene defect, absence of the placental enzyme would lead to interruption of pregnancy before the end of the first trimester[27,42].

It is therefore unclear whether decreased expression or function of human HSD3B1 might have pathological effects in the adult. Another important question is whether its increased expression or function might be associated with adult hyperaldosteronism. Although further clinical investigation will be needed to address this question, the identification of a zona glomerulosa–specific *HSD3B* gene subtype suggests a potential therapeutic application of subtype-specific HSD3B inhibitors. Historically, individuals with idiopathic hyperaldosteronism have been treated with a broad-spectrum HSD3B inhibitor that has negative side effects owing to its inhibition not only of aldosterone production but also of corticosterone synthesis[43,44]. It is thus tempting to speculate that selective inhibitors for the zona glomerulosa–specific HSD3B subtype may offer new therapeutic treatments for aldosterone control.

In conclusion, we have found an adrenalopathy in circadian clock–deficient *Cry*-null mice. The inactivation of *Cry* genes leads to chronically enhanced mineralocorticoid production, which, in turn, renders blood pressure salt-sensitive. Our analysis of the hyperaldosteronemia of these mice led to the discovery of a zona glomerulosa–specific HSD3B subtype. Although it is still not known how overproduced aldosterone causes salt-sensitive hypertension in *Cry*-null mice, our studies implicating this HSD3B isoform in hypertension may help unravel the etiologies of salt-sensitive hypertension and idiopathic hyperaldosteronism in humans.

METHODS

Methods and any associated references are available in the online version of the paper at http://www.nature.com/naturemedicine/.

Note: Supplementary information is available on the Nature Medicine website.

ACKNOWLEDGMENTS

We thank T. Ono, A. Hirasawa, T. Koshimizu, K. Terasawa, H. Nishinaga, M. Sato, Y. Yamaguchi, M. Matsuo, J.M. Fustin, K. Toida, H. Sei and K. Ishimura for technical support and valuable discussion. We also thank T. Michel for critical reading of the manuscript. This work was supported in part by the Specially Promoted Research (to H.O.) and Grant-in-Aid for Young Scientists (to M.D.) from the Ministry of Education, Culture, Sports, Science and Technology of Japan and grants from Nakatomi Foundation, SRF (to H.O.), Senri Life Science Foundation, Takeda Science Foundation (to M.D.) and the Netherlands Organization of Scientific research, ZonMW Vici 918.36.619 (to G.T.J.v.d.H.). Trilostane was a generous gift from Mochida Pharmaceutical. Eplerenone was a generous gift from Pfizer.

AUTHOR CONTRIBUTIONS

M.D. and H.O. designed the research; A.K., O.O., T.T. and G.T.J.v.d.H. supplied the experimental materials; M.D., Y.T., R.K., F.Y., H.Y., S.H., K.T. and H.O. acquired the data; M.D., N.E., Y.O., G.T., K.T. and H.O. analyzed the data; and M.D., G.T.J.v.d.H. and H.O. drafted the manuscript.

Published online at http://www.nature.com/naturemedicine/.
Reprints and permissions information is available online at http://npg.nature.com/reprintsandpermissions/.

1. Staessen, J.A., Wang, J., Bianchi, G. & Birkenhager, W.H. Essential hypertension. *Lancet* **361**, 1629–1641 (2003).
2. Lifton, R.P., Gharavi, A.G. & Geller, D.S. Molecular mechanisms of human hypertension. *Cell* **104**, 545–556 (2001).
3. Schibler, U. & Sassone-Corsi, P. A web of circadian pacemakers. *Cell* **111**, 919–922 (2002).
4. Dunlap, J.C. Molecular bases for circadian clocks. *Cell* **96**, 271–290 (1999).
5. Reppert, S.M. & Weaver, D.R. Coordination of circadian timing in mammals. *Nature* **418**, 935–941 (2002).
6. Wijnen, H. & Young, M.W. Interplay of circadian clocks and metabolic rhythms. *Annu. Rev. Genet.* **40**, 409–448 (2006).
7. Takahashi, J.S., Hong, H.K., Ko, C.H. & McDearmon, E.L. The genetics of mammalian circadian order and disorder: implications for physiology and disease. *Nat. Rev. Genet.* **9**, 764–775 (2008).
8. Panda, S. *et al.* Coordinated transcription of key pathways in the mouse by the circadian clock. *Cell* **109**, 307–320 (2002).
9. Green, C.B., Takahashi, J.S. & Bass, J. The meter of metabolism. *Cell* **134**, 728–742 (2008).
10. Hastings, M.H., Reddy, A.B. & Maywood, E.S. A clockwork web: circadian timing in brain and periphery, in health and disease. *Nat. Rev. Neurosci.* **4**, 649–661 (2003).
11. Furlan, R. *et al.* Modifications of cardiac autonomic profile associated with a shift schedule of work. *Circulation* **102**, 1912–1916 (2000).
12. Bradley, T.D. & Floras, J.S. Sleep apnea and heart failure: Part II: central sleep apnea. *Circulation* **107**, 1822–1826 (2003).
13. Scheer, F.A., Hilton, M.F., Mantzoros, C.S. & Shea, S.A. Adverse metabolic and cardiovascular consequences of circadian misalignment. *Proc. Natl. Acad. Sci. USA* **106**, 4453–4458 (2009).
14. van der Horst, G.T. *et al.* Mammalian Cry1 and Cry2 are essential for maintenance of circadian rhythms. *Nature* **398**, 627–630 (1999).
15. Vitaterna, M.H. *et al.* Differential regulation of mammalian period genes and circadian rhythmicity by cryptochromes 1 and 2. *Proc. Natl. Acad. Sci. USA* **96**, 12114–12119 (1999).
16. Matsuo, T. *et al.* Control mechanism of the circadian clock for timing of cell division in vivo. *Science* **302**, 255–259 (2003).
17. Yamaguchi, S. *et al.* Role of DBP in the circadian oscillatory mechanism. *Mol. Cell. Biol.* **20**, 4773–4781 (2000).
18. Kume, K. *et al.* mCRY1 and mCRY2 are essential components of the negative limb of the circadian clock feedback loop. *Cell* **98**, 193–205 (1999).
19. Okamura, H. *et al.* Photic induction of mPer1 and mPer2 in cry-deficient mice lacking a biological clock. *Science* **286**, 2531–2534 (1999).
20. Mitsui, S., Yamaguchi, S., Matsuo, T., Ishida, Y. & Okamura, H. Antagonistic role of E4BP4 and PAR proteins in the circadian oscillatory mechanism. *Genes Dev.* **15**, 995–1006 (2001).
21. Ishida, A. *et al.* Light activates the adrenal gland: timing of gene expression and glucocorticoid release. *Cell Metab.* **2**, 297–307 (2005).
22. Balsalobre, A. *et al.* Resetting of circadian time in peripheral tissues by glucocorticoid signaling. *Science* **289**, 2344–2347 (2000).
23. Young, W.F. Primary aldosteronism: renaissance of a syndrome. *Clin. Endocrinol.* **66**, 607–618 (2007).
24. Kaplan, N.M. Primary aldosteronism. in *Clinical Hypertension* 410–433 (Lippincott Williams & Wilkins, Philadelphia, 2006).
25. Brown, N.J. Eplerenone: cardiovascular protection. *Circulation* **107**, 2512–2518 (2003).
26. Gomez-Sanchez, C., Holland, O.B., Higgins, J.R., Kem, D.C. & Kaplan, N.M. Circadian rhythms of serum renin activity and serum corticosterone, prolactin and aldosterone concentrations in the male rat on normal and low-sodium diets. *Endocrinology* **99**, 567–572 (1976).
27. Simard, J. *et al.* Molecular biology of the 3β-hydroxysteroid dehydrogenase/Δ^5-Δ^4 isomerase gene family. *Endocr. Rev.* **26**, 525–582 (2005).
28. Payne, A.H. & Hales, D.B. Overview of steroidogenic enzymes in the pathway from cholesterol to active steroid hormones. *Endocr. Rev.* **25**, 947–970 (2004).
29. Giroud, C.J., Stachenko, J. & Venning, E.H. Secretion of aldosterone by the zona glomerulosa of rat adrenal glands incubated *in vitro*. *Proc. Soc. Exp. Biol. Med.* **92**, 154–158 (1956).
30. Domalik, L.J. *et al.* Different isozymes of mouse 11 β-hydroxylase produce mineralocorticoids and glucocorticoids. *Mol. Endocrinol.* **5**, 1853–1861 (1991).
31. Ogishima, T., Suzuki, H., Hata, J., Mitani, F. & Ishimura, Y. Zone-specific expression of aldosterone synthase cytochrome P-450 and cytochrome P-45011β in rat adrenal cortex: histochemical basis for the functional zonation. *Endocrinology* **130**, 2971–2977 (1992).
32. Rainey, W.E. Adrenal zonation: clues from 11β-hydroxylase and aldosterone synthase. *Mol. Cell. Endocrinol.* **151**, 151–160 (1999).
33. Potts, G.O., Creange, J.E., Hardomg, H.R. & Schane, H.P. Trilostane, an orally active inhibitor of steroid biosynthesis. *Steroids* **32**, 257–267 (1978).
34. Jungmann, E. *et al.* The inhibiting effect of trilostane on adrenal steroid synthesis: hormonal and morphological alterations induced by subchronic trilostane treatment in normal rats. *Res. Exp. Med. (Berl.)* **180**, 193–200 (1982).
35. Brown, R., Quirk, J. & Kirkpatrick, P. Eplerenone. *Nat. Rev. Drug Discov.* **2**, 177–178 (2003).
36. Mason, J.I. *et al.* The regulation of 3β-hydroxysteroid dehydrogenase expression. *Steroids* **62**, 164–168 (1997).
37. Makhanova, N., Hagaman, J., Kim, H.S. & Smithies, O. Salt-sensitive blood pressure in mice with increased expression of aldosterone synthase. *Hypertension* **51**, 134–140 (2008).
38. Rhéaume, E. *et al.* Structure and expression of a new complementary DNA encoding the almost exclusive 3β-hydroxysteroid dehydrogenase/Δ^5-Δ^4-isomerase in human adrenal glands and gonads. *Mol. Endocrinol.* **5**, 1147–1157 (1991).
39. Abbaszade, I.G. *et al.* Isolation of a new mouse 3β-hydroxysteroid dehydrogenase isoform, 3β-HSD VI, expressed during early pregnancy. *Endocrinology* **138**, 1392–1399 (1997).
40. Moisan, A.M. *et al.* New insight into the molecular basis of 3β-hydroxysteroid dehydrogenase deficiency: identification of eight mutations in the *HSD3B2* gene eleven patients from seven new families and comparison of the functional properties of twenty-five mutant enzymes. *J. Clin. Endocrinol. Metab.* **84**, 4410–4425 (1999).
41. Rhéaume, E. *et al.* Congenital adrenal hyperplasia due to point mutations in the type II 3β-hydroxysteroid dehydrogenase gene. *Nat. Genet.* **1**, 239–245 (1992).
42. Peng, L., Arensburg, J., Orly, J. & Payne, A.H. The murine 3β-hydroxysteroid dehydrogenase (3β-HSD) gene family: a postulated role for 3β-HSD VI during early pregnancy. *Mol. Cell. Endocrinol.* **187**, 213–221 (2002).
43. Nakada, T. *et al.* Primary aldosteronism treated by trilostane (3β-hydroxysteroid dehydrogenase inhibitor). *Urology* **25**, 207–214 (1985).
44. Winterberg, B., Vetter, W., Groth, H., Greminger, P. & Vetter, H. Primary aldosteronism: treatment with trilostane. *Cardiology* **72**(Suppl 1), 117–121 (1985).

ONLINE METHODS

Mouse experiments. The generation and breeding of *Cry*-null mice has been described previously[14,16,45]. Before experiments, we housed both WT and *Cry*-null mice for at least 2 weeks in a 12-h light-dark cycle to synchronize (entrain) the circadian clock of WT mice to the ambient light-dark cycle. We conducted all mouse experiments in constant darkness to eliminate a potential influence of external light on steroidogenesis[21] and to unequivocally define the effects of the internal biological clock. To eliminate gender- and age-related variations, we routinely used 12- to 16-week-old male mice. We transferred the mice into constant darkness, and at selected time points on the first day in constant darkness, we killed the mice to collect plasma and tissues. For pharmacological inhibition of 3β-HSD activity, we gave the mice a daily dose of 1.6 or 8.0 mg per kg body weight trilostane (a generous gift from Mochida Pharmaceutical), administered at 6–7 h after light onset by gavage as a suspension in 1% gum tragacanth. Seven days after the start of medication, we transferred the mice into constant darkness and collected plasma at CT0 in the dark. For salt-loading tests, we fed mice with one of the following diets (CREA Japan Inc.): a normal-salt diet containing 0.2% elemental Na^+, a high-salt diet containing 3.15% elemental Na^+ and a high-salt diet with the addition of eplerenone (a generous gift from Pfizer) at a concentration of 1.0 mg per g body weight in chow (estimated intake, 100 mg per kg body weight per d). All of the studies were approved by the Animal Experimentation Committee of Kyoto University.

Adrenal slice culture. Immediately after surgical isolation, we freed adrenal glands (one per assay) of adherent fat and cut them into four slices (about 0.4 mm thick) with fine scissors. We placed these four fresh slices in 1 ml of serum-free DMEM/F12 medium (Invitrogen), aerated with 5% CO_2, 95% O_2 at 37 °C. To wash out the serum carryover in the tissue slices, we preincubated them for 60 min at 37 °C under a 5% CO_2, 95% O_2 gas mixture shaking continuously at a rate of 150 cycles per minute. We replaced the preincubation medium with 1 ml of fresh serum-free medium and incubated the slices for 60 min under the same culturing conditions. We determined the amounts of aldosterone secreted into the medium by radioimmunoassay (Coat-A-Count Aldosterone kit, Siemens International).

Biochemical analysis of 3β-hydroxysteroid dehydrogenase-isomerase activity. We mechanically separated the adrenal glands into capsular and decapsulated portions according to the conventional method[29]. We determined 3β-HSD enzymatic activities in each portion as previously described[46]. We measured the conversion of [7-^{3}H]-pregnenolone (PerkinElmer) to ^{3}H-progesterone and the conversion of [1,2,6,7-^{3}H]-dehydroepiandrosterone (PerkinElmer) to ^{3}H-androstenedione. Briefly, we incubated cell extracts containing 5 μg of protein in reaction buffer (10 mM phosphate, pH 7.5, 140 mM NaCl, 4% propylene glycol) containing either 100 nM [^{3}H]-pregnenolone plus 10 μM pregnenolone or 100 nM [^{3}H]-dehydroepiandrosterone plus 15 μM dehydroepiandrosterone for 5 min at 37 °C. After incubation, we extracted steroids by ethyl acetate and subjected them to HPLC analysis by using a reversed-phase column, LiChrospher 100 RP-18 (4.0 mm × 250 mm; Kanto). We eluted the column with a 30-min linear gradient of 40–70% acetonitrile at a flow rate of 0.7 ml min^{-1}, followed by an isocratic elution of 70% acetonitrile. We fractionated the eluate every minute from 5 to 35 min and counted radioactivity in a liquid scintillation counter.

Taqman quantitative reverse-transcription PCR analysis of human *HSD3B1* and *HSD3B2*. We obtained human adrenalectomy specimens from Kyoto University Hospital with written informed consent. All human studies were approved by the Ethics Committee of Kyoto University Graduate School of Medicine. We collected cells in the zona glomerulosa or zona fasciculata separately by laser microdissection (**Supplementary Methods**). The high sequence similarity between human *HSD3B1* and *HSD3B2* (**Fig. 6a**) and the resultant potential cross-hybridization of their probes[38] were surmounted using Taqman MGB-containing fluorogenic probes, which can discriminate accurately between DNA fragments with only a few base pair mismatches[47]. We used the following Taqman probes: for *HSD3B1* (NM_000862.2), 5′-FAM-CCATACCCACACAGC-NFQ-MGB-3′ (NFQ is the nonfluorescent quencher) and for *HSD3B2* (NM_000198), 5′-VIC-TCCATACCCGTACAGCA-NFQ-MGB-3′. We amplified *HSD3B1* and *HSD3B2* cDNA fragments with F0 and R1 primers and with F0 and R2 primers, respectively (F0: 5′-AGAAGAGCCTCTGGAAAACACATG-3′, R1: 5′-TAAGGCACAAGTGTACAGGGTGC-3′; R2: 5′-CGCACAAGTGTACAAG GTATCACCA-3′). We added the Taqman probes for *HSD3B1* and *HSD3B2* together (250 nM each) to the reaction mixtures, as the use of different reporter dyes for each probe with separated emission wavelength maxima (probes for *HSD3B1* and *HSD3B2* are labeled with FAM and VIC, respectively) enabled simultaneous monitoring of *HSD3B1*- and *HSD3B2*-specific amplification in a single PCR tube. We performed real-time PCR with the StepOnePlus instrument (Applied Biosystems). We analyzed cDNA amplification curves with Sequence Detector software (Applied Biosystems), and we expressed the fluorescence of hybridized probes as ΔRn (normalized reporter signal). We normalized the expression of *HSD3B1* and *HSD3B2* to human *RPLP0* (NM_053275), which we evaluated by SYBR Green qPCR analysis (**Supplementary Methods**).

Statistical analyses. We analyzed the blood pressure changes of individual mice with the two-tailed paired Student's *t* test. For any other experiments in which three or more test groups were compared, we used one-way analysis of variance with Tukey's *post hoc* tests and evaluated the differences derived from genotypes, drug application and circadian time points tested.

Additional methods. Specific reagents and detailed methodology for the determination of PAC and PRA, DNA microarray analysis, isoform specification of *Hsd3b* and *Cyp11b*, promoter analysis of *Hsd3b6*, laser microdissection analysis of adrenal sections, *in situ* hybridization, immunohistochemistry, immunoblotting of adrenal microsomal extracts, qRT-PCR analysis of steroidogenic genes and radiotelemetric monitoring of blood pressure are all described in the **Supplementary Methods**.

45. Maeda, A. *et al.* Circadian intraocular pressure rhythm is generated by clock genes. *Invest. Ophthalmol. Vis. Sci.* **47**, 4050–4052 (2006).
46. Matsunaga, M., Ukena, K., Baulieu, E.E. & Tsutsui, K. 7α-hydroxypregnenolone acts as a neuronal activator to stimulate locomotor activity of breeding newts by means of the dopaminergic system. *Proc. Natl. Acad. Sci. USA* **101**, 17282–17287 (2004).
47. Kutyavin, I.V. *et al.* 3′-minor groove binder-DNA probes increase sequence specificity at PCR extension temperatures. *Nucleic Acids Res.* **28**, 655–661 (2000).